Adhesive Antibacterial Moisturizing Nanostructured Skin Patch for Sustainable Development of Atopic Dermatitis Treatment in Humans

Alicja Kosik-Kozioł[a], Paweł Nakielski[a], Daniel Rybak[a], Wiktoria Frączek[b], Chiara Rinoldi[a], Massimiliano Lanzi[c], Marta Grodzik[b], Filippo Pierini[a]*

a.　　　Department of Biosystems and Soft Matter, Institute of Fundamental Technological Research, Polish Academy of Sciences, Warsaw 02-106, Poland
b.　　　Department of Nanobiotechnology, Institute of Biology, Warsaw University of Life Sciences, Warsaw, Poland.
c.　　　Department of Industrial Chemistry "Toso Montanari", Alma Mater Studiorum University of Bologna, Bologna 40136, Italy

Abstract

Atopic dermatitis (AD) is a chronic, inflammatory skin disease with a complex etiology lacking effective treatment. The therapeutic goals include alleviating symptoms such as moisturizing and applying antibacterial and anti-inflammatory medications. Hence, there is an urgent need to develop a patch that effectively alleviates most of the AD symptoms. In this study, we employed a 'green' cross-linking approach of polyvinyl alcohol (PVA) using glycerol, and we combined it with polyacrylonitrile (PAN) to fabricate core-shell (CS) nanofibers through electrospinning. Our designed structure offers multiple benefits as the core ensures controlled drug release and increases the strength of the patch, while the shell provides skin moisturizing and exudate absorption. The efficient PVA cross-linking method facilitates the inclusion of sensitive molecules like fermented oils. *In vitro* studies demonstrate the patches' exceptional biocompatibility and efficacy in minimizing cell ingrowth into the CS structure containing argan oil, a property highly desirable for easy removal of the patch. Histological examinations conducted on an *ex vivo* model showed the non-irritant properties of developed patches. Furthermore, the eradication of *Staphylococcus Aureus* bacteria confirms the potential use of CS nanofibers loaded with argan oil and norfloxacin separately as an antibacterial patch for infected AD wounds. *In vivo* patch application studies on patients, including one with atopic dermatitis, demonstrated ideal patches' moisturizing effect. This innovative approach shows significant promise in enhancing life quality for AD sufferers by improving skin hydration and avoiding infections.

Graphical abstract (TOC)
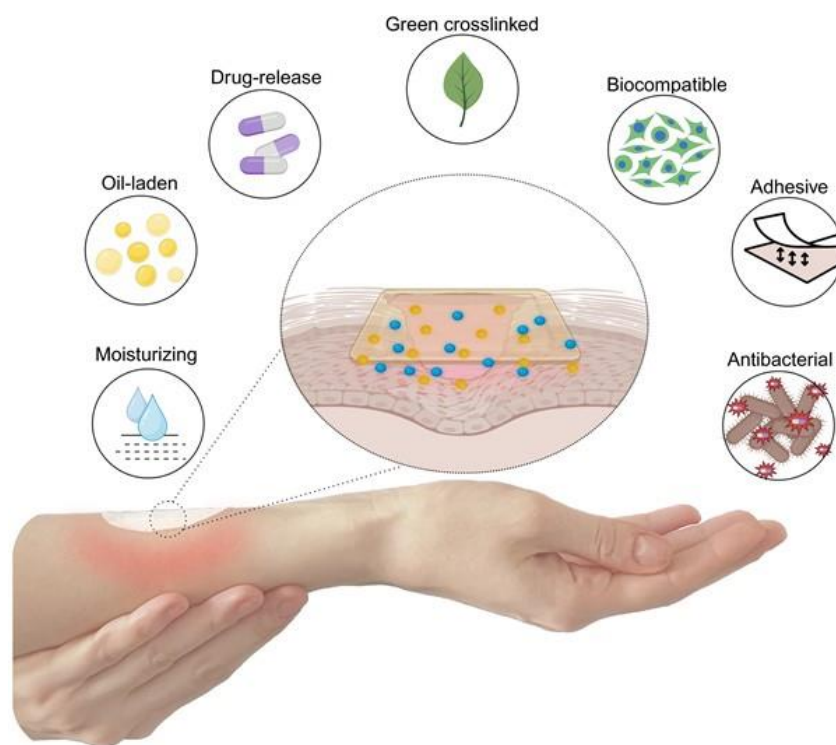
Introduction

Atopic dermatitis (AD, eczema) is an inflammation-based chronic disease affecting millions of individuals worldwide who genetically tend to overreact to external factors.[1] Eczema, prevalent in pediatric populations, strongly correlates with allergic rhinitis, asthma, or other atopic conditions. Its symptomatology includes intense itching, redness, dryness, papules, vesicles, and susceptibility to secondary infections.[2] Given the complex etiology of AD, there is no singular treatment approach for this condition. Topical corticosteroids are the initial treatment choice for this disease; nevertheless, their extended use may lead to dermal atrophy as an adverse effect.[3] Treatment objectives mitigating the symptoms of the condition encompass strategies such as skin hydration and barrier restoration with emollients, implementation of specific behavioral interventions to minimize scratching, utilization of antibacterial measures, and application of topical and/or systemic anti-inflammatory agents.[4]

Characterizing materials suitable for atopic dermatitis treatment should encompass features between those typically associated with bandages and wound dressings.[5] In eczema treatment, patches should ideally provide moisturization to counteract the inflammation caused by dry skin while also possessing characteristics such as softness, flexibility, elasticity, stress resistance, durability, and ease of handling. Various types of dressings, including electrospun nanofibers [6–8], biomaterial-based films [9], porous foams [10–13], functional hydrogels [10–13], and biological dressings [14,15] have been recently developed to expedite the skin healing process. Among these, hydrogels

have gained significant interest due to their ability to absorb wound exudate and maintain a moist environment at the wound sites.[16]

Poly(vinyl alcohol) (PVA) is a water-soluble, hydrophilic polymer with low toxicity, high water absorption, impressive mechanical properties, and excellent biocompatibility.[17-18] Traditional methods of cross-linking PVA involve the use of high or low temperatures (which can damage sensitive molecules) [19,20] or toxic chemicals, such as formaldehyde or glutaraldehyde (which can be irritating and potentially carcinogenic).[21,22] Herein, we employed eco-friendly cross-linking of PVA using glycerol (Gly) that can interact through hydrogen bonding, van der Waals forces, and hydrophobic interactions.[23] Green cross-linking offers several benefits compared to traditional approaches, such as: (1) eliminating the use of toxic chemicals, reducing the environmental impact and potential health hazards, (2) operating at room temperature, minimizing the risk of damaging sensitive molecules, or compromising the material's functionality as well as minimizing the final cost, which beneficially impacts on the fabrication scalability. The previous studies demonstrated that a PVA tough hydrogel could be achieved at room temperature by simply physically mixing PVA and Gly in water.[24] [25] Small molecular weight (SMW) molecules like Gly function as bridge molecules to connect PVA chains into bundles by forming many H-bonds with PVA chains and hence the formation of a gel network [25]. This method can be combined with salt such as NaCl to obtain the electrolyte, which exhibits impressive self-healing capabilities and moldability.[24] One study explored the potential of H-bonding in electrospinning, however, suboptimal process conditions necessitated the inclusion of cryo-gelation cross-linking.[23] In our research, we aimed to optimize conditions to fully utilize the potential of H-bonding between PVA and Gly, as described in the literature.[24,25]

Hydrogel nanofibers, while offering biodegradability and biocompatibility, often suffer from high hydrophilicity and poor mechanical strength, leading to deformation-prone dressings. By combining PVA hydrogels with synthetic polymers like polyacrylonitrile (PAN), patch properties can be enhanced. PAN, known for its strength and elasticity, has become a popular choice for developing bandages due to its excellent spinnability, promising mechanical properties, and potential for drug incorporation, thus promoting wound healing.[26,27]

Electrospinning has been employed to overcome the challenge of combining the hydrophilic and hydrophobic nature of these two polymers into a cohesive core-shell (CS) structure. Electrospinning represents a cost-effective and practical approach for the production of nanofibers characterized by attributes such as high porosity, small diameter, a remarkable strength-to-weight ratio, and a substantial surface-to-volume ratio.[28]

The developed patch for patients with atopic dermatitis can be further customized to individual patient needs by incorporating anti-inflammatory or antibacterial drugs, as well as skin-nourishing and moisturizing substances. One potential enhancement is the integration of plasmonic nanomaterials, which highlights its suitability for developing next-generation stimuli-responsive nanoplatforms implemented in biomedical applications such as bacterial infection[29], sensors[30], and on-demand drug delivery platforms[31]. Despite their excellent properties, some molecules can be damaged in contact with near-infrared light stimulation. Thus, more natural approaches should be developed. Plant extracts and isolated compounds are increasingly employed to alleviate symptoms and improve skin health in treating eczema. Argan oil and green tea oil are renowned for their moisturizing, nourishing, and anti-inflammatory properties.[32-33] The study involving rats with second-degree burns indicated that those treated with argan oil healed faster compared to those treated with silver sulfadiazine, a conventional burn treatment.[34] In cases where the skin is cracked, damaged, and infected due to eczema, incorporating such oils may provide relief.

Herein, we introduce a moisturizing, antibacterial, and adhesive eco-crosslinked CS nanofibrous skin patch designed for the treatment of AD. The PAN/PVA Gly fibrous matrix was fabricated through electrospinning using a co-axial needle system. We evaluated the material's performance with various commonly used drugs, including anti-inflammatory drugs (Ibuprofen, Ketoprofen, Dexketoprofen), glucocorticoid (Dexamethasone), non-opioid analgesic agents (Paracetamol), and broad-spectrum antibacterial antibiotic (Norfloxacin). Comprehensive investigations were conducted on the physicochemical and mechanical properties of the CS system, as well as its *in vitro* performance with fermented argan and green tea oils. Moreover, we assessed the antimicrobial efficacy of argan oil and Norfloxacin-loaded CS fibers. The study also includes in-depth histological examinations, and the final patch applicability was proved by *in vivo* tests conducted on humans, including patients with both normal skin as well as suffering from eczema.

RESULTS AND DISCUSSION

For individuals with eczema, it's crucial that the dressing not only absorbs wound exudate but also ensures moisturization. This study aimed to develop an adhesive, antibacterial, and skin-moisturizing nanofibrous patch **(Figure 1a)**. We fabricated multifunctional nanofibrous materials through the electrospinning process of the CS nanofiber system, based on PVA-Gly (shell) and PAN (core) presented in **Figure 1b**. The outer part of the patch was functionalized with fermented oils using a method that avoids the use of destructive crosslinkers **(Figure 1c)**. Additionally, the patch was modified with the inclusion of anti-inflammatory or antibacterial drugs to address multiple needs in the treatment of atopic dermatitis wounds **(Figure 1d).**

Initially, we engineered environmentally friendly PVA hydrogel nanofibers, excluding typical toxic crosslinkers for this polymer, and mitigated the risk of high/low temperatures that could potentially degrade the incorporated oils. To address this concern, Gly was chosen as the cross-linking agent for PVA. PVA and Gly can undergo various intermolecular interactions, including hydrogen bonding, van der Waals forces, and hydrophobic interactions. PVA, a water-soluble polymer with numerous hydroxyl (-OH) groups in its structure, engages in hydrogen bonding with water and other molecules possessing H-bonding capabilities.[23] Similarly, Gly, being a hydrophilic molecule with three hydroxyl groups, can also form hydrogen bonds with water and other molecules. When PVA is combined with Gly, the hydroxyl groups in PVA can establish hydrogen bonds with the hydroxyl groups in Gly. This leads to the formation of intermolecular cross-links between these two molecules, resulting in increased mechanical strength and elasticity of the resulting material.[23–25] The schematic representation of the green-crosslinking process of PVA using Gly is illustrated in **Supporting information, Figure S1a**. Gly acts as a plasticizer, enhancing the mobility of the polymer chains. This increased mobility facilitates the alignment and formation of crystalline regions within the material, further contributing to its mechanical strength while reducing its solubility.[25] Furthermore, the addition of Gly to PVA stabilizes and facilitates the dispersion of oil particles in the solution, as shown in **Supporting Information, Figure S2a.** In the solution without Gly, oil particles separate from the solution and float on its surface to form an oil-water interface, while upon the addition of Gly, a homogeneous solution forms with small particles that completely integrate with the polymer after electrospinning **(Supporting Information, Figure S2b)**.

As widely known, non-crosslinked PVA electrospun nanofibers tend to completely dissolve immediately after placing in water at room temperature. Gly cross-linking method effectively preserved the integrity of the nanofibers over the testing period **(Supporting Information, Figure S2c)**. To verify the effectiveness of our cross-linking method, we conducted solubility tests over one month and examined the fiber morphology before and after the tests. SEM images displayed cylindrical, continuous PVA-Gly nanofibers with random orientation and a smooth surface without visible beads **(Supporting information, Figure S3a)**. After one month of immersion in water, the SEM images of the mats demonstrated that the fibers were preserved, providing evidence that the Gly cross-linking process was successful **(Supporting information, Figure S3b)**. However, it was apparent that the fibers had started to slightly degrade, which is a natural process for this polymer.[35]

Henceforth, the green-crosslinked PVA networking system was implemented to fabricate an advanced CS fibrous structure with potential fabrication scalability and product commercialization. CS fibers were generated by incorporating a co-axial dispensing into the electrospinning process using liquid polymer solutions. This method takes advantage of the electrospinning solutions' ability to undergo rapid cross-linking upon exposure to voltages. Simultaneously dispensing hydrophobic PAN and hydrophilic PVA-Gly solutions through the inner and outer needles of the co-axial needle, respectively, results in the formation of CS fibers. Subsequently, these fibers are collected in layers on the collector. SEM imaging was conducted to evaluate the morphology of core-shell fibers. CS exhibits well-defined cylindrical, continuous, and defect-free nanofibers with a smooth surface **(Figure 1e)**. Comparing the morphologies of PVA-Gly fibers **(Supporting information, Figure S3a)** and CS fibers **(Figure 1e, Supporting information Figure S3c)**, it is evident that the latter sample type has a better-defined morphological structure. Similarly to PVA-Gly, the impact of the aqueous environment on the CS fiber morphology was examined over a month, and it was observed that there was no change in their morphology during this period **(Supporting information, Figure S3d).** This indicates that the addition of PAN stabilizes the material's structure. The average diameter of CS fibers is 309,8±77,72 nm **(Figure 1e).** CS nanofiber mat exhibits an average porosity of 30%, facilitating gas exchange. The CS patch is thin yet possesses a large surface area with slight variations in thickness (160,16 µm ± 20,23 µm). However, these differences do not significantly impact its functionality. Thin design ensures sufficient gas transportation through the wound and appropriate drug release. The large surface area obtained through the electrospinning method allows the patch to maintain its thin structure while effectively absorbing wound exudate. This design is particularly beneficial for treating atopic dermatitis, as it maintains a moist wound environment and ensures efficient drug delivery, which is essential for effective treatment. Following this, fiber orientation analysis was performed using the OrientationJ plugin in ImageJ. The analysis method employs a pixel-wise algorithm to calculate a 2D structure tensor, generating, among others, coherency maps and orientation. The orientation of each pixel corresponds to the direction of the largest eigenvector of the tensor, weighted by its coherency, which is defined as the ratio between the difference and the sum of the tensor eigenvalues.[36] A coherence structure for the CS nanofibers has been achieved, indicating consistent alignment and uniformity in the fiber structure **(Supporting information, Figure S3c)**. This coherence suggests a well-organized and controlled fabrication process, enhancing the overall quality and integrity of the material. **Figure 1f** depicts a hue-saturation-brightness (HSB) color map of the analyzed SEM image of CS nanofibers. The electrospun nanofibers possess an overall random orientation, albeit with a predominant alignment towards 45 and 60 degrees **(Figure 1f)**. A TEM study was conducted to verify whether the employed co-axial needle system functions in

terms of CS structure organization as intended. TEM images display visible boundaries between the core (PAN) and shell (PVA-Gly), providing evidence of the CS structure **(Figure 1g)**.
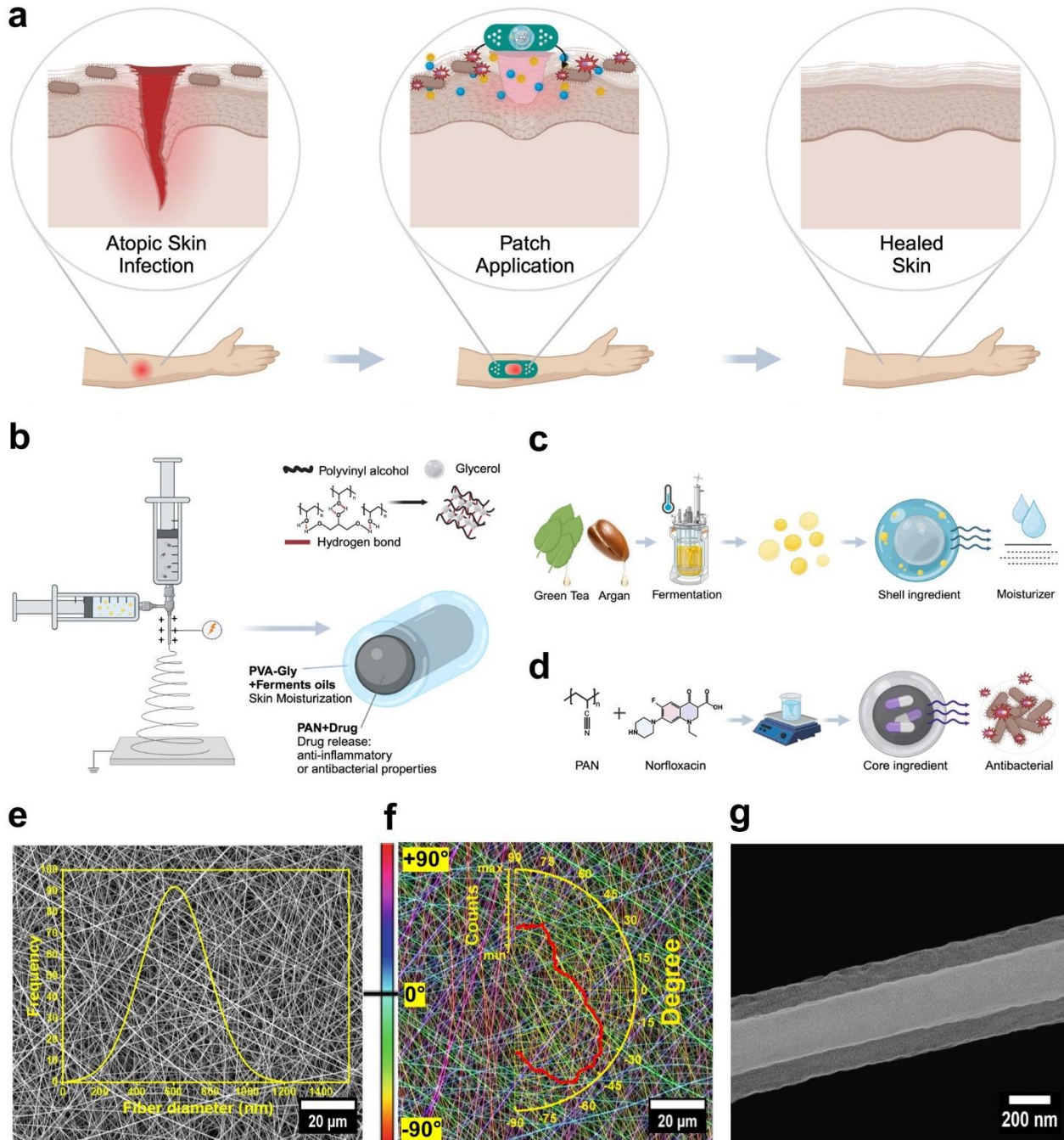
Figure 1. Multifunctional AD skin patch topical application, design, and fabrication. (a) *Schematic illustrations presenting the application for eczema wound healing with the moisturizing mucoadhesive and antibacterial patch. **(b)** Co-axial electrospinning set-up schematic representation of the CS fibers designed for atopic dermatitis wound care. PVA used for the shell part undergoes green cross-linking with* Gly *(PVA-Gly) through the formation of hydrogen bonds. PAN was applied as a core part of CS. **(c)** CS functionalization with fermented oils in PVA-Gly shell to nourish and moisturize skin. **(d)** CS embedding antibacterial (or anti-inflammatory) drugs loaded in PAN core to heal the wound bed. **(e)** SEM micrograph*

presenting CS electrospun nanofibers with diameter distribution. (f) CS HSB color-coded map with the circular histogram of fiber local orientation. (g) TEM images of a CS nanofiber revealing the development of the requested CS nanostructuration.

Surface analysis via ATR-FTIR was employed to examine the chemical composition and functional groups present on the materials' surfaces. **Figure 2a** presents a comparison of the spectra of CS fibers along with their constituent elements, including both the core (PAN) and the shell (PVA-Gly). Furthermore, to meticulously investigate the bonding processes facilitated by the environmentally friendly cross-linking method utilized for PVA-Gly, we juxtaposed it with its non-crosslinked counterparts: electrospun PVA fibers (PVA) and Gly (**Supporting Information, Figure S4a**). The peak at 3660 cm^{-1} in the ATR-FTIR spectrum of PAN nanofibrous mat is typically associated with the stretching vibration of the N-H bond. The peaks at 2976 cm^{-1}, 2927 cm^{-1}, 1458 cm^{-1}, and 1398 cm^{-1} are related to vibrations of the aliphatic CH groups: CH, CH_2, and CH_3. The presence of a weak peak at 1668 cm^{-1} in the ATR-FTIR spectra, associated with the C=O bond, indicates the residual existence of DMF in the PAN fibers due to incomplete evaporation during the electrospinning process.[37] The peak around 1243 cm^{-1} in the ATR-FTIR spectrum of PAN is attributed to the stretching of the C-N bond in the amide group. ATR-FTIR of Gly solution revealed a wide peak at 3280 cm^{-1} indicating O-H stretching. The 2923 cm^{-1}, 2890 cm^{-1}, and 1423 cm^{-1} peaks are due to asymmetric and symmetric stretching and bending vibration of the CH_2 group, respectively (**Supporting Information, Figure S4a**). The peaks of 1107 cm^{-1} and 1023 cm^{-1} are from the stretching of C-O in CHOH, while the 920 cm^{-1} band is from the stretching of C-O in CH_2OH.[38] ATR-FTIR spectra of PVA electrospun mat show main peaks at 3280 cm^{-1}, 2919 cm^{-1}, 1696 cm^{-1}, 1419 cm^{-1}, 1113 cm^{-1}, 1030 cm^{-1}, 929 cm^{-1} (**Supporting Information, Figure S4a**) corresponding to O-H stretching vibration of hydroxyl group, CH_2 asymmetric stretching vibration, C=O carbonyl stretch, C-H bending vibration of CH_2, C-H deformation vibration, C-O stretching of acetyl groups and C-C stretching vibration, respectively.[39] In the case of the combination of PVA and Gly (PVA-Gly), the peak which indicates the formation of bonds between them, is the peak associated with the stretching vibration of the -OH bond. This peak in the ATR-FTIR spectrum of the PVA-Gly blend shows a shift compared to the individual spectra of PVA and Gly (from 3280 cm^{-1} to 3318 cm^{-1}), suggesting mutual interactions and the formation of hydrogen bonds between the hydroxyl groups of both components. This is a typical phenomenon for polymer and compound mixtures capable of forming hydrogen bonds. Moreover, similar peaks were observed in the spectrum, but with a notable enhancement at a wavelength of 2920 cm^{-1}. This enhancement suggests a stronger interaction or bonding between the functional groups present in PVA and Gly. The ATR-FTIR spectra of CS reveal the presence of characteristic peaks corresponding to the shell, thus confirming the CS structure, which is consistent with previous findings in the literature.[17,40]

The thermal degradation behavior of CS and its individual components (e.i., PVA-Gly and PAN) was studied by TGA, and it is presented in **Figure 2b**. For PVA-Gly, there is a noticeable decrease in sample weight caused by the loss of water below 110°C. The second rapid mass loss is observed in the range 110-255°C, which is attributed to the decomposition and degradation of the PVA-Gly components. The visible change in mass is observed around 200°C, which is associated with the complete decomposition of Gly. The full degradation of PVA is observed up to 450°C. For the PAN group, we can observe the first rapid decline step began at 260°C and ended at 320°C, which was attributed to the volatile products produced by PAN pyrolysis, such as NH_3, CH_3CN, and HCN. The second stage of PAN decomposition occurred between 320 and 470°C. The TGA curve for CS

exhibits a consistent decrease in weight loss, aligning with the behavior of its constituent parts, thus confirming the presence of all investigated components in the system.

X-ray patterns for CS, PVA-Gly, and PAN electrospun fibrous mats are shown in **Figure 2c**. The XRD analysis of the pure PVA fibrous mat exhibited prominent crystalline reflections at approximately $2\theta = 19.50°$ (**Supporting Information, Figure S4b**), distinctive of PVA and representing reflections from the (101) planes within a monoclinic unit cell.[41] In the XRD profile of the PVA-Gly nanocomposite fibrous mat, the intensity of the PVA diffraction peak decreased and appeared broader than in pure PVA (**Figure 2c**). This observation can be attributed to the presence of crystallinity alongside a significant amount of diffuse scattering, indicating the co-existence of PVA nanocrystalline phase with the bulk amorphous phase.[42] As the amorphous nature increases, the intensity of the XRD pattern for PVA decreases.[43] The amorphous nature results in greater diffusivity, which is characteristic of amorphous polymers possessing a flexible backbone. This confirms changes in the behavior of PVA fibrous mats, which, from a relatively rigid material, become fully flexible upon the addition of Gly, acquiring the ability to deform and return to their original shape after distortion in an aqueous environment. In the pristine PAN nanofibers, a crystalline peak centered around 17° is attributed to the PAN polymer phase.[44] In the case of CS, we observe two peaks typical for PVA-Gly and PAN, unequivocally confirming that the fibrous mat consists of PAN core coated with PVA-Gly.

The developed CS possesses remarkable stiffness, expressed through a high Young's Modulus of 42.9±14.0 MPa, a crucial aspect in maintaining the dressing's stability over the wound site **(Figure 2d,e)**. Furthermore, its elongation at a break of 16.8% is equally essential, rendering it highly flexible **(Figure 2f)**. CS groups exhibit impressive uniformity in resisting tensile forces, achieving a tensile strength of 2.5±0.4 MPa **(Figure 2g)**. Both the shell and core components have similar tensile strengths (2.6±0.7 MPa and 2.8±0.3 MPa, respectively). This means that our CS structure ensures consistent resistance to stretching forces throughout the dressing. Moreover, the designed fibrous dressing possesses notable mucoadhesive properties, with a force of adhesion measuring 2.25±0.3 N **(Figure 2h)** and mucoadhesion of 205±12.9 μJ **(Figure 2i)**. These metrics reflect a high level of stickiness and bonding strength, which are crucial attributes for an effective wound dressing. In comparison to the data available in the literature regarding mucoadhesive dressings, the developed CS system exhibits very good mucoadhesive properties.[45–47] The mucoadhesion value indicates the energy required to detach the dressing from the wound surface, showcasing its capability to adhere firmly to biological tissues. The obtained force of adhesion demonstrates a robust ability to maintain contact with the wound bed, providing secure and reliable coverage for improved healing outcomes **(Figure 2j)**. Similar adhesion tests to the finger were conducted for electrospun PVA-Gly and PAN mats, as presented in the **Supporting information, Figure S5a,b.** These nanofibrous mats exhibit high adhesion to the finger, maintaining this effect consistently during bending at 0-45-90 degrees. This further validates the results of mucoadhesive tests. Additionally, the adhesion of the CS patch to other substrates was tested, exemplified by its adhesion to nitrile gloves, which also confirmed the high mucoadhesive properties of the designed patch (**Supporting information, Figure S5c**). The adhesion of the patch to the skin involves several physical and chemical mechanisms that ensure effective attachment and therapeutic efficacy. Van der Waals forces, which are weak, non-covalent interactions occurring between the molecules of the adhesive and the skin, significantly contribute to the overall adhesion strength despite their individual weakness. [48] Additionally, hydrogen bonding plays a crucial role as the

adhesive forms hydrogen bonds with the skin's surface, which contains proteins and water molecules capable of acting as hydrogen bond donors and acceptors, thereby enhancing the patch's adhesion. [49] Furthermore, mechanical interlocking occurs when the adhesive's physical structure penetrates the microscopic contours and pores of the skin, creating a mechanical bond that further enhances adhesion. Cohesive forces within the adhesive material maintain its integrity, ensuring that it remains intact during both application and removal. [50] By leveraging these mechanisms, our patch achieves robust and reliable adhesion to the skin. Thanks to its elastic properties and even stress distribution, developed dressing minimizes skin irritations and inflammations. This combination of exceptional stiffness and flexibility makes the CS a reliable choice for wound dressings that require both stability and the ability to adapt to body movements, contributing to comfortable wear.
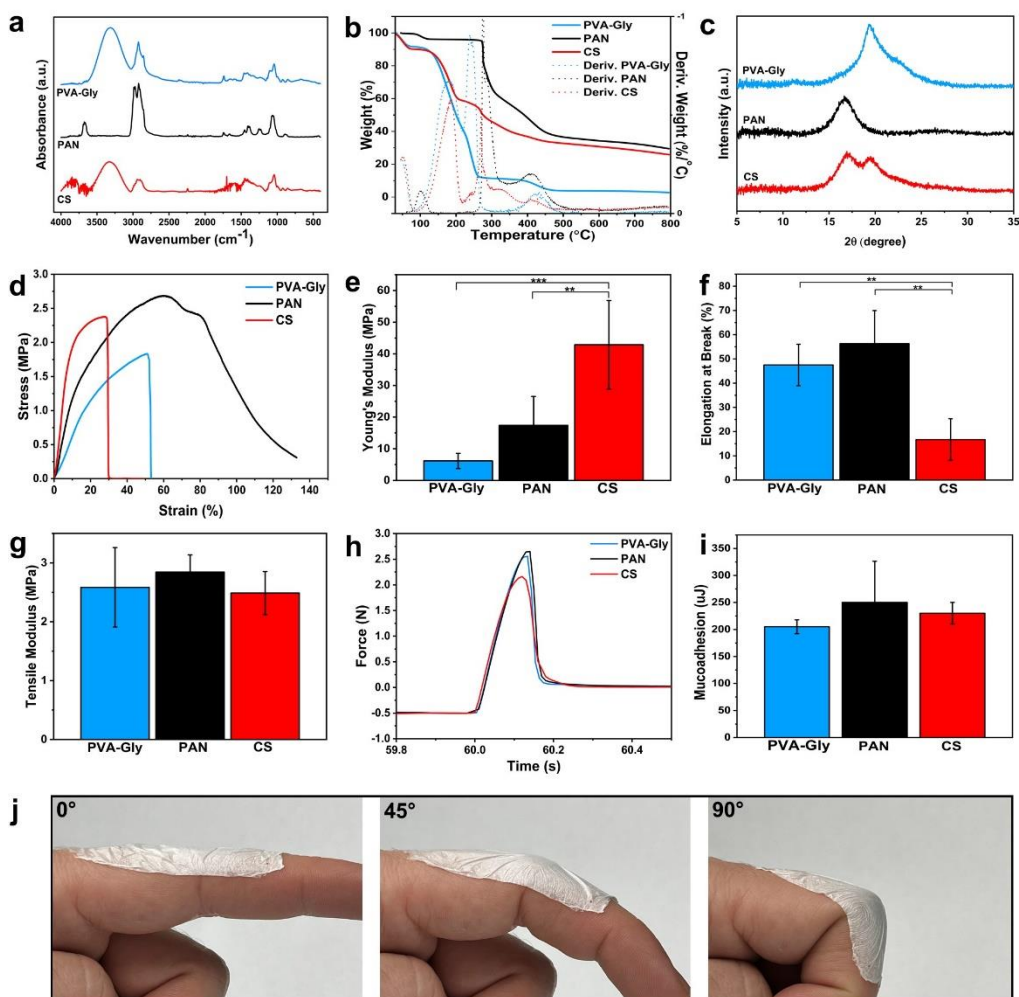
***Figure 2. Physico-chemical and mechanical characterization of CS nanofibers composing the patch, as well as monolithic PVA-Gly and PAN reported as references**. (**a**) ATR-FTIR spectra (**b**) TGA thermograms comparing weight percentage to temperature, and (**c**) XRD diffractograms for the monolithic fibers and* CS. *(**d**) Stress-strain curves, (**e**) Young's modulus, (**f**) elongation at break, (**g**) tensile modulus, (**h**) force of adhesion, and (**i**) mucoadhesion (P-value <0.01 (**), <0.001 (***)). (**j**) Application of the CS patch on the finger illustrating the strong material adhesion during bending at 0°, 45°, and 90° positions.*

As mentioned before, PVA-Gly mats exhibit remarkable elasticity Gly, added to the PVA solution, acts not only as a cross-linking agent stabilizing PVA but also as a plasticizer, increasing the flexibility of polymer chains. Differences in the flexibility of PVA-Gly, PAN, and CS fibers, apart from water tests, are also evident in the appearance of the mats themselves **(Figure 3a)**. PVA-Gly is highly flexible and elastic, PAN resembles separate cotton-wool fibers, while CS exhibits properties between these two, achieving optimal characteristics. The water contact angle test was conducted on electrospun mats to assess their wettability properties, as shown in **Figure 3b**. The shell, made of PVA-Gly, displayed a contact angle of 22.2±1.6 degrees, indicating highly hydrophilic characteristics. In CS system, where the shell coated the highly hydrophobic PAN core (97.4±1.8 degrees), the contact angle increased to 36.8±2.2 degrees, suggesting a suitable substrate for water-based applications. PAN mat, despite being highly hydrophobic upon direct contact with water, loses this property and exhibits highly absorbent characteristics after surface wetting. PAN is a polymer that contains nitrile groups in its chemical structure. These groups are generally considered moderately polar. Upon exposure to water or aqueous solutions, nitrile groups can undergo partial hydrolysis, forming amide or carboxylic acid groups, which are more hydrophilic. After initial contact with water, the microstructure of the PAN surface may change, leading to an increase in areas available for interaction with water. This phenomenon can also include the expansion or opening of pores within the material, enhancing its ability to absorb water. [51–54] The material, in appearance and behavior, resembles cotton wool as depicted in **Figure 3a**. The objective of the developed CS structure is for use as an eczema dressing. Wound dressings serve multiple functions including fluid absorption to manage exudate, promotion of moist wound healing, prevention of maceration, enhancement of comfort, and reduction of infection risk. Thus, the absorption properties of the developed material have been thoroughly evaluated **(Figure 3c)**. Each component was studied individually to comprehensively understand the fluid absorption behavior within CS structure. All fiber types reach a saturation point after 120 minutes of testing. The developed green-crosslinked network of PVA-Gly offers a significant advantage with its limited water absorption. This characteristic is attributed to the substantial amount of Gly present within the fiber's interior. Such absorption properties are highly desirable for hydrogel fibers. Conversely, as mentioned before, the monolithic PAN fibers exhibit impressive water absorption, which may lead to adverse effects such as drying out the wound and potentially delaying the healing process. However, as observed in the swelling curves, combining this material with a hydrogel coating leads to a shift in absorptive properties. Thus, the CS structure demonstrates anticipated fluid absorption capabilities, allowing the wound to remain consistently moist while efficiently absorbing excess exudate. Both excessive and insufficient fluid absorption would fail to meet the requirements of wound dressings, underscoring the importance of designing dressings with appropriate absorption properties. During the degradation analysis of the electrospun mats, notable mass loss was observed in the hydrogel water-soluble biodegradable PVA-Gly, reflecting a natural degradation process. The semicrystalline PAN exhibited the slowest degradation rate and demonstrated an initial stage of significant water absorption (0-3 days), followed by gradual degradation **(Figure 3d)**. The observed increase in the mass of PAN fibers in the first 3 days of the degradation experiment can be explained by the combination of initial water uptake and swelling

behavior of PAN fibers. We ensured the drying process was thorough, but slight residual moisture could still be a factor. In detail, during the first few days, when PAN fibers absorb water, partial hydrolysis of nitrile groups in PAN to form more hydrophilic amide or carboxyl groups leads to a temporary increase in mass.

In CS configuration, the inclusion of synthetic PAN in the core resulted in an extension of the degradation period compared to the hydrogel material used independently (e.g., PVA-Gly).

For dressings containing therapeutic substances, ensuring optimal release timing is crucial. Dressings should be left on the skin for approximately 3-24 hours. For applications lasting longer than 3 hours, the dressing should be moistened approximately every 2–3 hours.[55–58] To enhance user convenience and avoid the need for frequent moistening, our goal was to develop a material that would remain on the skin for 3 hours while releasing the contained medication during this time. Moreover, in the treatment of atopic dermatitis, minimizing the risk of wound infection is paramount hence a 3-hour application period is considered optimal. The developed CS system provides different drugs that can be released for up to 120 hours, as depicted in **Figure 3e**. During the investigation of CS drug release in a water-based environment, it was noted that there exists a relationship between the atomic mass of the drug chemical compound and its release behavior from the fibers. The release behavior of a drug from fibers is significantly influenced by various factors, including its molecular mass, crystallinity, solubility, composition, hydrophilicity, and degradation rate.[59] As presented in **Figure 3e**, smaller molecules tend to have greater mobility and can release more rapidly, while bigger molecules may face challenges in penetrating fiber structures, impacting the rate and intensity of release. As a result, we observe the decreased release with increasing molecular mass in the following order: Ibuprofen (Mw: 206.28 Da), Ketoprofen (Mw: 254.28 Da), Norfloxacin (Mw: 319.40 Da), Dexketoprofen (Mw: 375.42 Da), and Dexamethasone (Mw: 392,46 Da). To thoroughly examine the impact of the CS structure and its components on the release profile, we conducted a case study using Ibuprofen (IBU) as the drug that exhibited the highest release rate among the tested drugs. These studies were conducted on IBU release from fibers made solely of the shell's material, as well as monolithic core's materials, and compared them with the developed CS structure **(Figure 3f)**. To minimize the possible and unwanted impact of the fiber dimension effect on the drug release rate, the three mentioned fibers were produced with similar fiber size distributions. Due to its internal structure, the overall release rate of CS fibers was significantly slower compared to monolithic fibers, which is in line with the typical trend documented in the literature.[17] Additionally, the release trend of CS fibers steadily increased during the initial 6 hours of incubation.
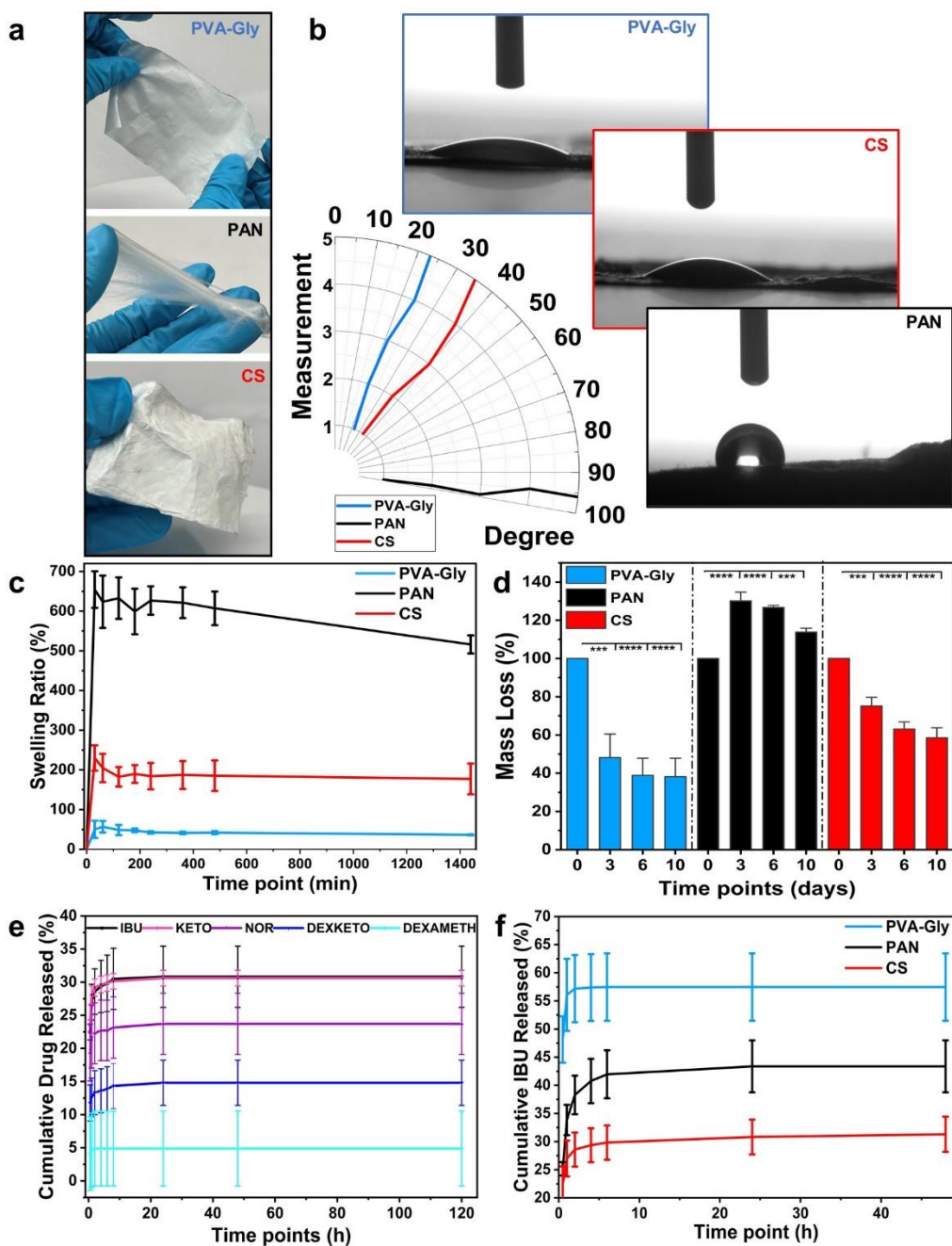
Figure 3. Nanoplatform behavior in an water environment. (a) *Photos of PVA-Gly, PAN, CS nanofibrous mats. (**b**) water contact angle of CS, PVA-Gly, and PAN nanofibers. (**c**) Nanofiber swelling up to 24h of incubation in PBS solution. (**d**) Nanofiber degradation presenting a change of sample mass up to 10 days of incubation in PBS solution. (**e**) Cumulative release of drugs: Ibuprofen (IBU), Ketoprofen (KETO), Norfloxacin (NOR), Dexketoprofen (DEXKETO), Dexamethasone (DEXAMETH) from CS fibers. (**f**) Comparison of Ibuprofen release from CS, PVA-Gly, and PAN nanofibers.*

We opted to functionalize our developed CS system with a range of fermented oils, well-known for their dual advantages in the skincare sector. These oils not only strengthen the skin's inherent protective barriers, helping to preserve optimal moisture levels and guard against moisture loss,

12

but also assist in alleviating skin irritations. To preserve targeted concentrations of the developed CS, we experimented with different concentrations of fermented oil additives within the shell layer. This particular layer was selected to optimize the oil's interaction with the patient's skin. We tested oil concentrations ranging from 5% to 15%, determining that the maximum concentration capable of producing accurate fibers without beads was 10% **(Supporting Information, Figure S6a)**. The average fiber diameter values with oil additives do not significantly deviate from the CS diameter, as depicted in **(Supporting Information, Figure S6b)**.

To assess the biocompatibility of the proposed fibrous matrices, their interaction with L929 fibroblast cells was investigated. Firstly, we conducted standard direct cell seeding tests on CS fibrous materials and CS with argan oil (CS-A), green tea (CS-G), and the combination of these two oils (CS-AG). As a control, cells were seeded on standard cell culture well plates **(Figure 4a)**. L929 cells were properly grown on the scaffolds, and an increase in their proliferation was observed from day 1 to day 7. On the 7th day of incubation, it was observed that scaffolds containing a combination of green tea and argan oils (CS-AG) led to significantly lower cell proliferation compared to pure oils and the controls **(Figure 4b)**. The lower cell proliferation observed on scaffolds with a combination of oils could stem from complex interactions between oil components, altered bioactivity, or the presence of inhibitory compounds, underscoring the need for deeper exploration. Loading one type of oil into the CS structure is feasible, and the system is compatible, but the proliferation results indicate that the pristine CS exhibits better cell development properties. In the development of a skin dressing, having a fully biocompatible material is crucial; however, equally important is its ease of detachment from the skin. Cell proliferation results indicate that a surface rich with oily components slows down cell proliferation. For patches, this property is highly desirable, as it restricts the proliferation of healed tissue onto the bandage, enabling its easy removal. Simultaneously, the material remains entirely biocompatible with the patient body. Balancing these two important properties, it is observed that CS-A is a good candidate for application on wounds, thus, this material was further examined. Utilizing electron microscopy micrographs, morphological analysis was performed on day 3 of culture. L929 cells exhibited spreading, assuming an elongated, spindle-like morphology, highlighting the efficient support for cell adhesion and spreading. Notably, no significant differences were observed among the various tested conditions, suggesting the absence of mutagenic or pathological changes **(Figure 4c)**. Culturing cells on materials provides a cellular response stimulated by the topography of biomaterial surfaces as well as by the compounds released from them. To exclude the surface influence and investigate solely the impact of the substances, in vitro tests were conducted indirectly by treating cells with extracts from the developed dressings **(Figure 4d)**. Extracts from selected nanofibers (CS and CS-A) significantly stimulate cell growth and proliferation compared to pure cell culture medium (TCP), as depicted in **Figure 4e**. For the indirect test, a Live/Dead assay was employed, marking cells in green or red to indicate their live or dead state. Live/Dead images demonstrated a considerable majority of viable green cells on day 7 of culture, indicating high cell viability and all materials' cytocompatibility **(Figure 4f).** Visualization using a confocal microscope was utilized to assess the morphology of the actin cytoskeleton and cell nuclei performed on day 3 of incubation. L929 cells treated with CS-A and CS extracts maintained proper morphology typical for that stage of incubation time **(Figure 4g)**.
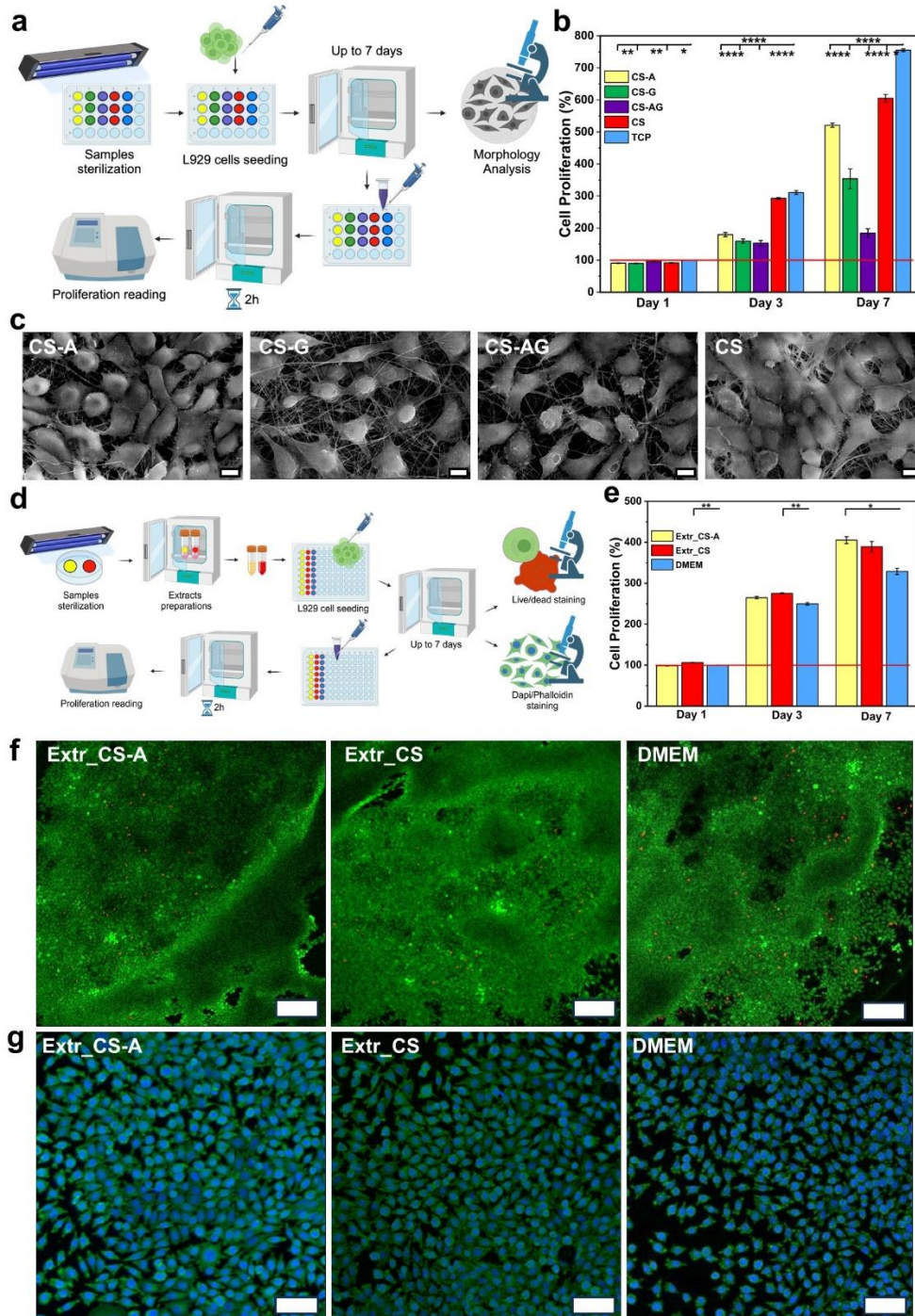
***Figure 4. In vitro L929 cell biocompatibility.** (**a**) Illustration presenting direct cell seeding test. (**b**) Cell Proliferation from direct study: cells seeded on the CS, CS loaded with fermented oils: CS-A: core-shell with argan oil, CS-G core-shell with green tea oil, CS-AG core-shell with argan+green tea oils, and control TCP (Tissue Culture Plastic). (**c**) SEM images of cell-seeded scaffolds after 3 days of incubation, scale bar equal to 10 µm. (**d**) Illustration presenting indirect cell test, using extracts from the CS-A and CS nanofibers (Extr_CS-A, Extr_CS and normal medium without extracts (DMEM). (**e**) Cell Proliferation from indirect study. (**f**) Live/Dead tests after 7 days of incubation. Live cells are stained green, while dead cells are red, scale bar equal to 200 µm. (**g**) Immunostaining after 3 days of cell incubation, scale bar equal to 100 µm.*

14

To further investigate the potential application of the selected CS and CS-A materials as skin dressings, *ex vivo* tests were conducted. The EpiDerm™ model is cultivated at an air-liquid interface, forming a multilayer structure resembling the human epidermis but lacking certain cell types like melanocytes, Langerhans cells, or Merkel cells. Despite this, it is an optimal model for skin toxicity testing.[60-61] This multilayer structure comprises the stratum corneum layer (CL), granular layer (GL), spinous layer (SL), and basal layer (BL), as illustrated in **Figure 5a**. To quantitatively assess and evaluate CS and CS-A biocompatibility, cellular metabolic response (MTT) was conducted **(Figure 5b)**. Following the MTT assay to assess tissue metabolism, the next step involved determining the activity of lactate dehydrogenase (LDH) in the culture media **(Figure 5c)**. This sequence of tests enables a comprehensive analysis of metabolic activity, where the MTT assay provides information on tissue's ability to reduce substrates, whereas LDH confirms enzymatic activity indicative of intermediate metabolism.[62-63] To validate the method's reliability, a positive control - PC (SDS treatment) yielded negative results in all parameters tested, confirming the method's accuracy. It is important to underscore the significance of the fact that the optimal exposure time-point for the Epiderm tissue model was determined to be 18 hours, as per the extensive optimization carried out in the literature for the Epiderm skin irritation test (EPI-200-SIT-MD).[64] The MTT assay conducted on tissues, which evaluated mitochondrial activity, indicated that both CS and CS-A exhibited no irritant potential. The viability of keratinocytes in the 3D model remained statistically unchanged compared to the negative control – NC (treated with DPBS). The positive control, treated with a solution exhibiting strong irritant properties, showed approximately 5.5% cell viability in the EpiDerm™ model, relative to the negative control. Similarly, results were obtained in the LDH assay, which was used to assess the level of cell membrane damage in the cell population. Analysis of cell media collected after treating EpiDerm™ with polymer extracts yielded a similar percentage level as those treated with DPBS (NC). On the contrary, the leakage of LDH into cell medium in tissues treated with a 1% SDS solution showed a four-fold increase in values compared to the negative control. A comprehensive evaluation of the biocompatibility of polymers also included morphological analysis. Conducting H&E staining as part of this study allowed for the assessment of the condition of all layers of the examined tissues **(Figure 5d)**. In both CS and CS-A instances, all layers of the epidermis are visible and adequately stained in both control tissues (treated with DPBS) and those subjected to the action of extracts from both tested polymers. The observed tissue images depict loosely connected cells, characteristic of the outer stratum corneum, as well as keratohyalin granules that normally appear ranging from rounded to star-shaped in the granular layer. The spinous layer exhibited flat cells, as expected, whereas the basal layer cells displayed columnar shapes with rounded contours. In none of the cases presented, changes indicative of an inflammatory process were detected. Conversely, tissues exposed to SDS showed a distinct outcome. These EpiDerm™ samples exhibited numerous irregularities, such as non-uniform morphology in the stratum corneum and signs of damage indicative of necrosis, affirming the irritant properties of the substance employed.
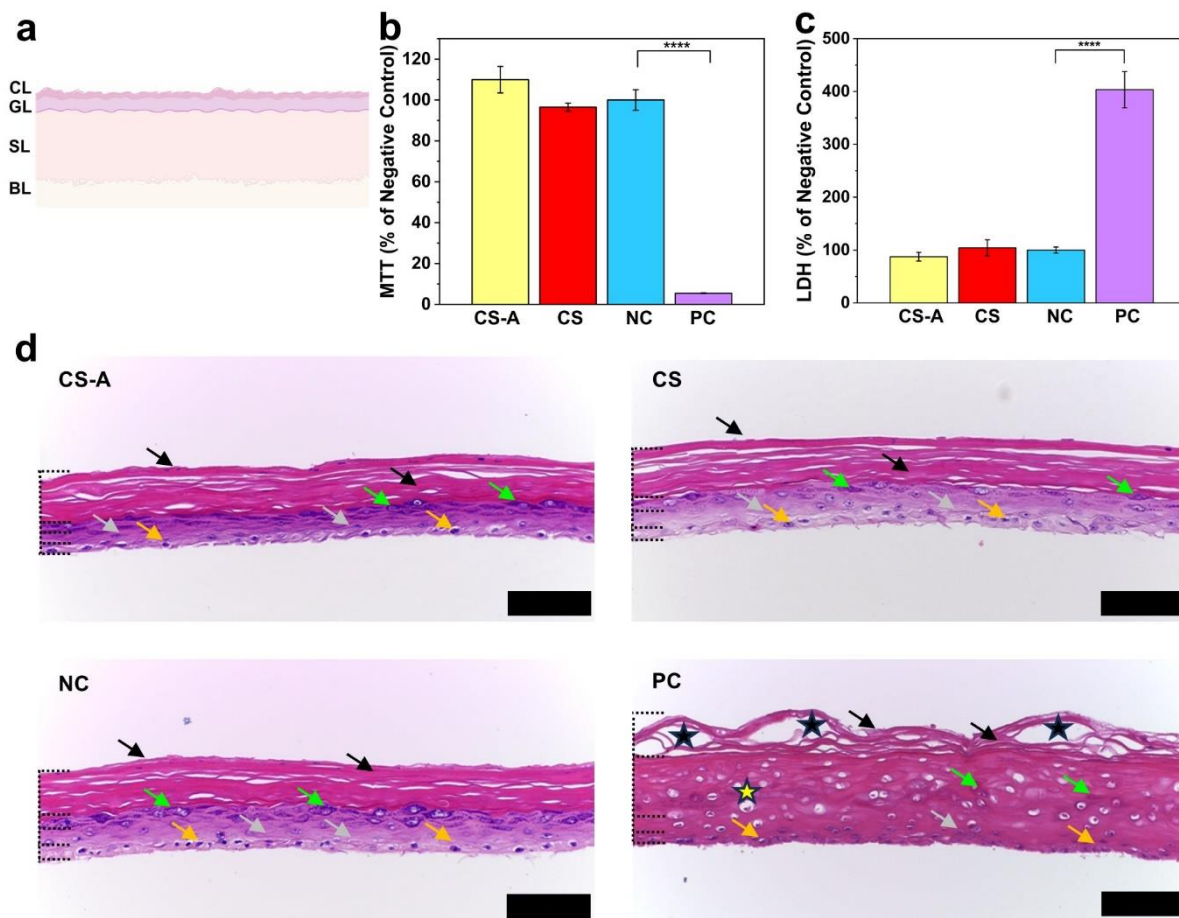
***Figure 5. Histological examination using EpiDerm^TM. (a)** Schematic of tissue structure composed of corneal layer (CL), granular layer (GL), spinous layer (SL), and basal layer (BL), respectively. **(b)** EpiDerm^TM viability evaluated by the MTT assay. **(c)** Cytotoxicity evaluated by LDH assay. **(d)** Tissue visualization after H&E staining. The following cells are indicated by arrows: black – the loosely arranged cells of stratum corneum, green – lamellar bodies with keratohyalin granules, grey – flattened cells of spinous layer, orange – the basal layer cells with a columnar shape with rounded contours. Stars indicated: black - damaged tissue, yellow – presents of necrosis. Mean ± standard deviation values are presented. Statistical significance between control and treated cells is indicated by an asterisk, evaluated using Tukey's multiple comparison test (p < 0.05). Asterisks (****) represent p < 0.0001. Abbreviations: NC, negative control (DPBS treated); PC, positive control (1% SDS treated); CS and CS-A, tissues treated with polymer extracts. Scale bars equal to 100μm.*

Considering the high occurrence of infections in patients with eczema wounds, designed CS significantly contribute to eliminating bacteria commonly found in the epithelial environment. We examined the bacterial inactivation on nanofibrous samples with (CS-A) and without fermented oil (CS), as well as with the commonly utilized antibacterial drug named norfloxacin (CS-NOR). We utilized *Staphylococcus aureus*, the predominant causative agent of primary skin infections in humans.[65] The selection of this bacterial strain was primarily motivated by its frequent colonization of the skin in patients with atopic dermatitis, a factor contributing to the onset and worsening of AD symptoms.[66]

Figure 6a presents a detailed depiction of the sequential agar plate methodology employed to assess the performance and effectiveness of the developed materials. During the standard procedure, the fibrous samples were kept in the agar plates inoculated with bacteria for 24 h in the incubator. The antibacterial effect of the oil-loaded samples (CS-A) was not noticeable. The explanation for this occurrence is that CS-A, when placed on a solidified agar plate and incubated at 36°C for 24 hours, does not excrete oils from its structure, thus failing to hinder bacterial growth. As expected, bacteria colonized the entire plate for both positive (CS) and negative (CTRL, bacteria plate itself) controls. Norfloxacin release from CS (CS-NOR), unlike argan oil, effectively penetrates the agar plate, inhibiting bacterial growth, with the observed inhibition zone measuring an average diameter of 3.29 ± 0.2 cm (**Figure 6b**). However, wounds commonly maintain a moist environment due to wound exudate. Therefore, a quantitative test was conducted in liquid conditions to simulate such an environment, as illustrated in **Figure 6c**. During the test, the antibacterial effect was assessed by holding a bacterial solution of 10^6 bacteria in contact with investigated fibrous nanofibers for 3 hours, which is the planned application contact time of the dressing with the wound bed. Afterward, a quantitative analysis of bacterial dilutions was measured by placing these solutions on agar plates and incubating them for 24h. The quantitative analysis shows that bacteria survival decreased to 33.62 ± 6.3 % and 36.04 ± 5.8 % for argan oil and norfloxacin, respectively (**Figure 6d**).
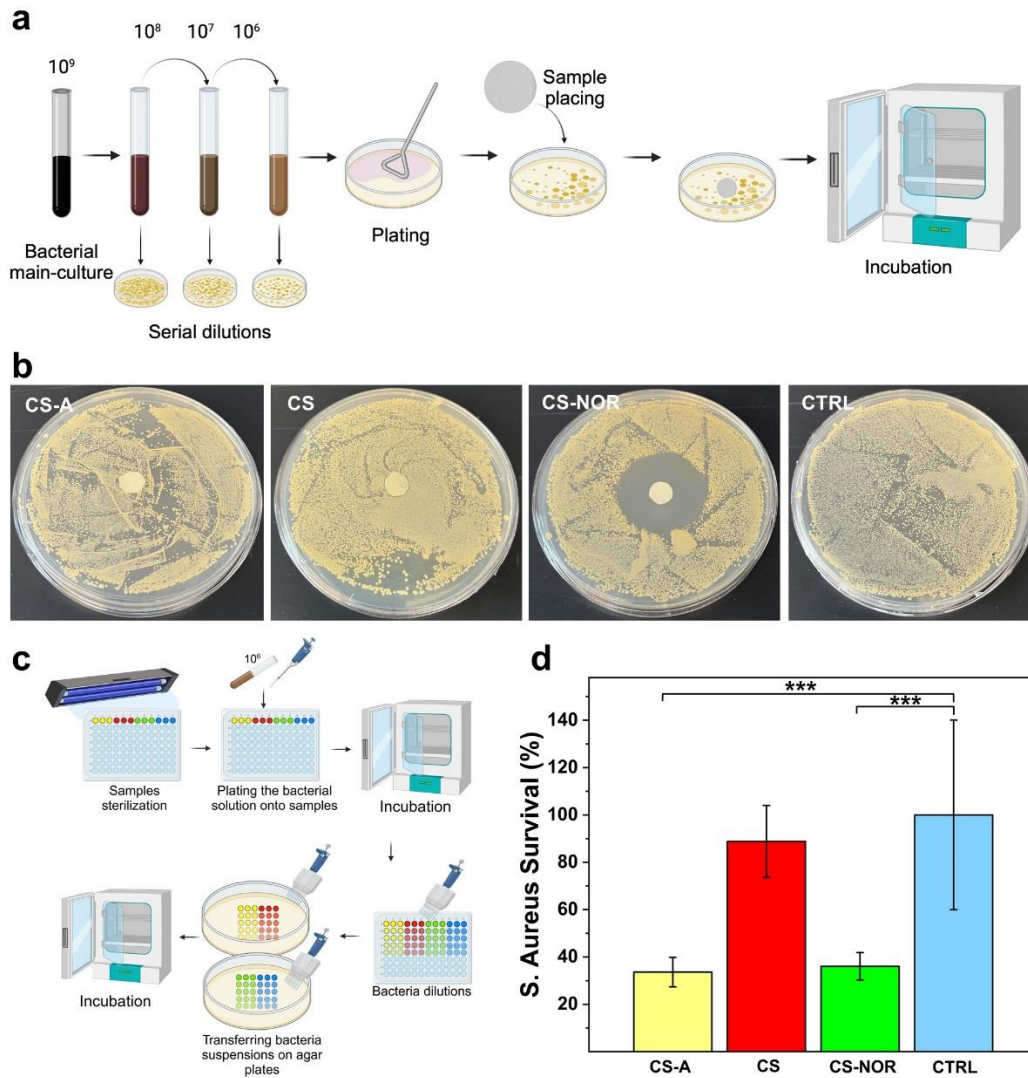
Figure 6. Antimicrobial efficacy of developed nanoplatforms. (a) Sketch presenting a qualitative disk diffusion study of the electrospun fibers. (b) Photos of Staphylococcus aureus colonies growing on LB agar plates on which fibrous nanofibers were placed for each tested condition: core-shell with norfloxacin (CS-NOR), core-shell (CS), core-shell with argan oil (CS-A), control bacteria colony (CTRL) one day after incubation. (c) Schematic presenting a quantitative test for measuring bacteria killing efficiency. (d) Quantitative survival of Staphylococcus aureus after 3h liquid-contact with nanofibers.

After a comprehensive characterization of the material's biocompatibility and antimicrobial properties, targeted *in vivo* application tests were performed on the selected CS and CS-A patches. The developed skin patches were also compared with commercially available gauze dressings (as purchased and added with argan oil). Volunteers representing diverse geographic locations and skin types, including 5 Poles, 2 Italians, and 1 Iranian, participated in the evaluation of patches designed with four different types of dressings (Group 0: untreated skin; Group 1: dry Gauze; Group 2: gauze soaked with argan oil; Group 3: CS; Group 4: CS-A (**Figure 7a** and **Supporting Information, Figure S7**). The skin hydration level was evaluated by measuring the degree of hydration before and after the application of the tested dressing groups, following the

manufacturer's instructions for the skin analyzer (**Supporting Information, Figure S7a**). To monitor the environmental impact on the skin throughout the experiment, Group 0 served as the skin reference, where no dressing was applied. Different areas of the hand's skin exhibit varying moisture levels, and although the skin's moisture level was measured at a reference site, each hand region was assessed before applying the respective patches to accurately represent the actual moisture level influenced by the tested material. At this point, it is important to note the adhesion of dressings to the skin. Similarly to the previous patch adhesion test, the adherence of CS-A, the gauze, and gauze soaked with argan oil to the fingertip was assessed during bending at 0, 45, and 90 degrees (**Supporting Information, Figure S5d-f**). CS-A shows comparable adhesion to the CS patch. Plain gauze exhibits no adhesion, while gauze soaked with oil adheres to the finger; however, the oil drips off the dressing, and during bending to 90 degrees, it detaches from the surface of the finger. Thus, to ensure consistent permeability and stability conditions for all dressings throughout the entire application study, the patches were secured in the same manner using tape (**Supporting Information, Figure S7b**). It is crucial to emphasize the comfort of wearing the patches containing oils, such as those in groups 2 and 4, where the developed CS-A shows significant advantages. Unlike oil-saturated gauze, it is a product that does not stain clothing and comes ready for use, as it already contains oil within itself, thereby eliminating the necessity for additional oil application (**Supporting Information, Figure S7c,d**). Moisture measurements were taken at 3 and 6 hours post-patch application, with 5 records taken for each measurement (**Figure 7a**). After 3 hours of wearing the patches, it was observed that CS performed the best, with a total increase in hydration of 78% across all patients, which further increased to 89% after 6 hours of wearing (**Figure 7a**). Patient no. 1 suffers from advanced eczema and exhibits typical symptoms associated with this condition, including itching, dry skin, and very often redness and flaky skin. In 7 out of 8 participants tested, the CS dressing demonstrated impressive moisturizing efficacy. Among all patients, excluding patients no. 6 and 7, significant improvement in skin moisture was observed after 6 hours of wearing the CS-A dressing (**Figure 7b** and **Supporting Information, Figure S7e**). For patient no. 1, who suffers from eczematous skin, we find that the CS-A patches are markedly more effective than saturating gauze with the same oil. For this specific patient, the CS dressing was most effective when worn for 3 hours. However, considering the longer wear time (6 hours), CS-A turns out to be a slightly better material, which requires a longer time to nourish the skin. As we observe, eczema-affected skin is highly sensitive to environmental changes (**Figure 7b** and **Supporting Information, Figure S7e**). Real-time measurements (Group 0, Patient 1) after 3 hours reveal a significant increase in skin hydration, likely influenced by various factors such as washing, temperature changes, etc. Given this understanding, addressing such dermatological concerns is considered exceptionally vital and intricate. Our dressing endeavors to transport therapeutic compounds deep within the nanofiber structure, simultaneously maintaining proper skin hydration through the outer oil-coated shell. Demonstrating significant efficacy, developed dressings effectively moisturize the skin, even for the patient, necessitating specialized care. After removing the dressings, no skin changes, irritations, or allergic symptoms were observed in any patient (*Supporting Information, Figure S7f*). Considering the patch application test results, the CS patch exhibited the highest average hydration levels for all patients, achieving 78% after 3 hours of wear and 89% after 6 hours. Following closely behind is the CS-A patch, which appears to be the preferable choice for some patients (Patients 1, 2, 5).
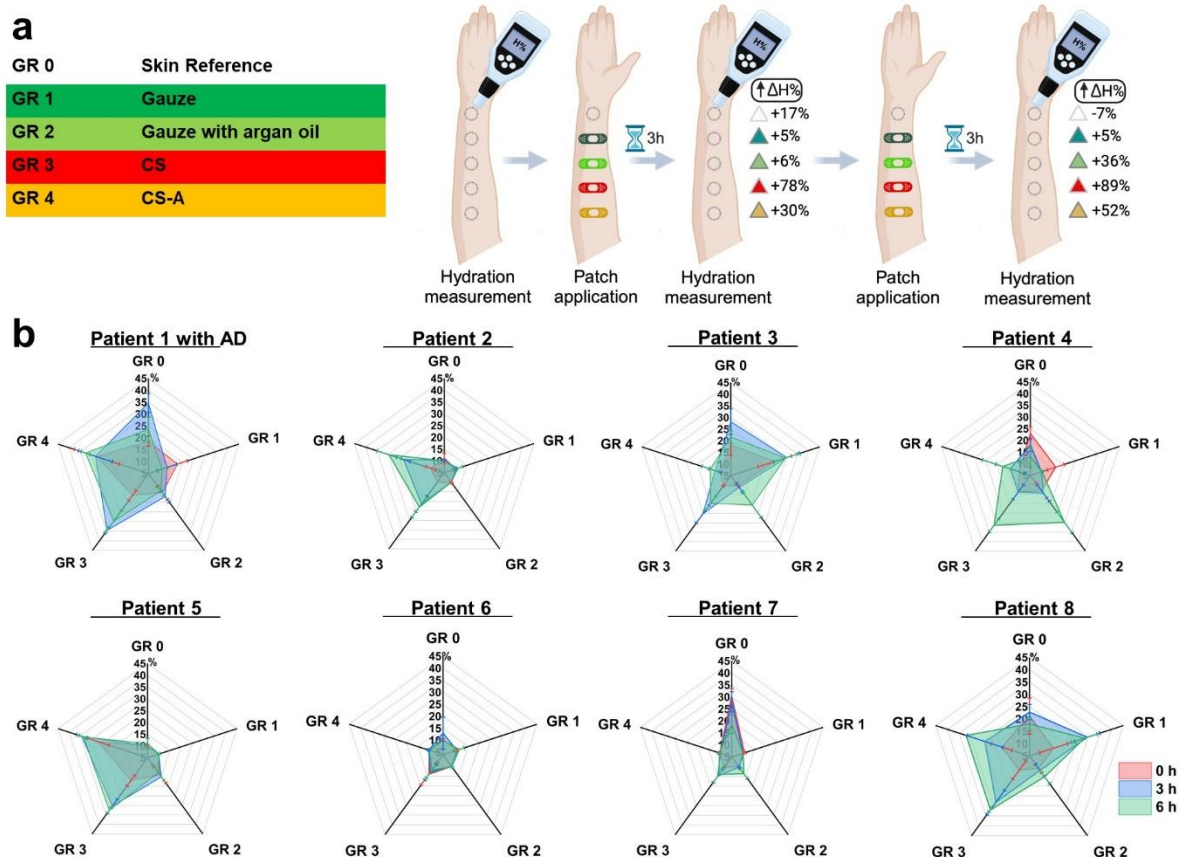
Figure 7. In vivo skin patch application tests on humans. *(**a**) Illustration presenting the skin hydration test performed using LCD Minimo digital skin condition analyzer. Four types of patches were tested (Group 0: untreated skin; Group 1: dry Gauze; Group 2: gauze soaked with argan oil; Group 3: core-shell (CS); Group 4: core-shell with argan oil (CS-A)). Records for each group were done in five replicates: before patch application (0h), in the middle of measure time (after 3h), and at the end of patch application (6h). The summarized values indicating the overall effectiveness of skin hydration for each tested group were calculated as the average across all participants. (**b**) Skin hydration for 8 individual patients after 0 hours, 3 hours, and 6 hours of nanostructured patch application. Patient no. 1 suffers from atopic dermatitis (AD, eczema).*

CONCLUSIONS

In summary, we developed skin-moisturizing adhesive antibacterial patches for patients with atopic dermatitis. The optimized assembling and integration of PAN/PVA-Gly/fermented oils/drugs as a CS nanofiber-based platform endow the patch with advanced multifunctionality. The CS skin patches facilitated fluid absorption capabilities, allowing a wound to remain consistently moist while absorbing excess exudate. The developed patches exhibit suitable flexibility and stiffness, which are crucial for maintaining dressing stability over the wound site. Additionally, it boasts remarkable mucoadhesive properties reflecting superior stickiness and bonding strength essential for effective wound care. The applied PVA green-crosslinking opens a window for the usage of sensitive molecules such as fermented oils, avoiding the destructive crosslinkers' affection. The developed CS patch is a completely biocompatible platform for cell growth and proliferation.

Additionally, besides remaining biocompatible, CS supplemented with argan oil possesses a specific surface that reduces the predisposition of cell proliferation ingrowth into the patch. Furthermore, leveraging the drug delivery function of the nanostructured patch enables customization to address the specific requirements of eczema patients by integrating appropriate anti-inflammatory or antibacterial agents. The eradication of *Staphylococcus Aureus* bacteria in the water-based environment confirms the potential application of CS-A and CS-NOR as antibacterial patches in infected wounds. In-depth histological examinations conducted on EpiDerm™ model confirmed the non-irritant properties of developed patches. The final patch's applicability, as demonstrated by *in vivo* tests conducted on humans, including patients with both normal skin and those suffering from atopic dermatitis, indicates that the developed nanofibrous platform exhibits outstanding moisturizing properties without causing skin irritations. Our CS stands out as a multifunctional and biocompatible nanofibrous platform, offering the release of multiple drug types alongside outstanding physicochemical and application properties. This versatility positions it not only as an effective treatment option for the demanding condition of atopic dermatitis but also as a viable solution for addressing various other skin disorders such as acne, seborrheic dermatitis, burns, sores, and skin mycosis.

METHODS

Materials

Polyvinyl alcohol (PVA) with an average molecular weight (Mw) in the range of 85 000-124 000 Da and a degree of hydrolysis (DH) of 99+%, polyacrylonitrile with an average Mw 150 000 Da, glycerol for molecular biology ≥99%, phosphate buffer saline (PBS), hexamethyldisilazane (HMDS), Triton X-100, 4′,6-Diamidino-2-phenylindole dihydrochloride (DAPI), sodium dodecyl sulfate, 3-(4,5-dimethylthiazol-2-yl)-2,5-diphenyltetrazolium bromide (MTT), Ibuprofen, Ketoprofen, Dexketoprofen Tromethamine, Dexamethasone, and Norfloxacin were obtained from Sigma-Aldrich. N, N-dimethylformamide (DMF) was obtained from Roth. Ethanol was purchased from Chempur. Dulbecco's modified Eagle's medium (DMEM), fetal bovine serum (FBS), penicillin-streptomycin (PS), and EDTA-trypsin were bought from Gibco Invitrogen. Alexa Fluor 488 Phalloidin and Live/Dead assay were purchased from Thermo-Fisher Scientific. Fermentoil Green Tea (Labio) seed and fermentoil Argan (Labio) were kind gifts from Erbslöh Polska. Viscoplast Sterile gauze dressing (3M) was obtained from the pharmacy. EpiDerm™ (EPI-200), reconstructed human epidermal tissues was sourced from MatTek Corporation (Ashland,). The CytoScan LDH Cytotoxicity Assay kit was obtained from G-Bioscience. Lysogeny broth (LB) and lysogeny agar (LB agar) were obtained from A&A Biotechnology. Gram-positive bacteria *Staphylococcus aureus (S. aureus)* ATCC 6538 was obtained from Pol-AURA.

Solution Preparation

PVA Green-Crosslinkable Shell Solution Optimization. To implement environment-friendly, non-toxic green cross-linking, we formulate PVA-Gly solutions. We investigate different concentrations varied between 6-10% (w/v) PVA concentration and 8-10% (v/v) Gly for electrospinning application. The optimal selected procedure was the following: PVA was dissolved in Mili-Q deionized water to obtain 8% w/v and stirred at 90°C for 3h until complete dissolution. Afterward, the solution was mixed overnight. Gly was added to the PVA solution to

obtain 10% v/v 2h before electrospinning. Immediately before electrospinning, ethanol was added to the polymer mixture in a volume ratio of 1:9.

Core and Shell Electrospinning Solutions. For the shell solution, we use the same formulation as the one described in the previous paragraph. Whereas, the core solution was prepared by dissolving 10% w/v PAN in DMF.

Drug-loaded CS Nanofiber Solutions. Core solutions (10% w/v PAN in DMF) were mixed overnight with different commonly used nonsteroidal anti-inflammatory drugs (Ibuprofen, Ketoprofen, Dexketoprofen), glucocorticoid (Dexamethasone), non-opioid analgesic agent (paracetamol) and broad-spectrum antibacterial antibiotic (Norfloxacin), separately, to obtain 5% w/v drug concentration.

Fermented oils-laden CS Nanofiber Solutions. The shell solution (PVA-Gly) was blended with fermented oils, including argan and green tea, at a concentration of 10% v/v. Moreover, a combination of both at a concentration of 5% each was tested.

Nanostructured Patch Fabrication

Electrospinning of Monolithic PVA Nanofibers for Green-Crosslinking Optimization. To investigate the PVA green-crosslinked nanofibers, we loaded PVA-Gly solution to the 1 mL syringe with a 22G, equal to an internal diameter (ID) of 0.413 mm. The syringe was lodged into a syringe pump dispensing the polymer solution with a flow rate of 620 μL/h, and it was connected to a high voltage power supply generating a potential of 16.5 kV The solutions were spun onto a flat collector at a distance of 18 cm from the needle. The electrospinning process was conducted under ambient conditions with a temperature of 20°C and humidity of 45%.

CS Nanofiber Fabrication. Solutions were loaded into 1 mL plastic syringes and dispensed simultaneously in a core/shell fashion through a two-coaxial needles system. The core and shell solutions were simultaneously dispensed through the inner (21G, ID = 0.514 mm) and outer needles (15G, ID = 1.372 mm), respectively, with a flowing rate of 620 μL/h. The co-axial needle was connected with 16.5 kV voltage. The solutions were spun onto a flat collector at a distance of 18 cm from the co-axial needle to obtain defect-free electrospun mats of a thickness of around 90 μm.

Morphological and Physico-Chemical Characterization

Electron Microscopies. Electrospun mats were visualized using scanning electron microscopy (JSM-6010PLUS/LV, In TouchScope microscope) at a working distance of 10 mm and 15kV accelerating voltage. Before imaging, nanofibers were coated with a 7 nm gold-sputtered layer in a DII-29030SCTR JEOL Smart Coater. To precisely determine the CS structure of the fibers, transmission electron microscopy was performed. For TEM analysis, electrospinning was performed directly on a TEM grid, then sputtered with 7 nm gold. TEM studies were conducted using the ZEISS Crossbeam 350 microscope at a working distance of 2 mm and an accelerating voltage of 30kV.

Spectroscopies and Thermal Analyses. An attenuated total reflectance Fourier transform infrared spectroscopy (ATR-FTIR) analysis was conducted to validate the structure of PVA-Gly, PAN, and CS. Additionally presented in *Supporting information* were PVA (Pure PVA fibers without cross-linking) and Gly (solution). The measurements were carried out using the attenuated total reflectance (ATR) technique on an Alpha-II BRUKER spectrometer equipped with diamond crystal, with each sample undergoing 32 scans within the 400 to 4000 cm^{-1} range, followed by averaging. X-ray diffraction (XRD) analysis was conducted using a Bruker D8 Discover

diffractometer, operating at 40 kV and 40 mA, equipped with a Cu anode (λ = 1.5406 Å). The measurements were carried out in reflection mode, following the Bragg–Brentano geometry, utilizing a Goebel mirror with a deflection of 0.677 degrees, a 1 mm slit, and two Soller collimators with an axial divergence of 2.5 degrees. The sample underwent ten scans at a high sampling rate for each specific temperature step, with a duration of 0.045 seconds per data point and an angular resolution of 0.04 degrees in the 2θ range of 0-35 degrees.

Thermogravimetric analysis (TGA) was conducted with a Q5000 (TA Instruments) instrument employing a nitrogen atmosphere. Thermogravimetric measurements were carried out in the temperature range of 20-800 °C to analyze the PVA-Gly, PAN, and CS nanofibers mats, each weighing approximately 3 mg. The analysis of TGA data was carried out utilizing TA Universal Analysis software, and consistent heating was maintained at a rate of 20 °C/min for all measurements.

Mechanical Characterization

Tensile Tests. To examine the suitability of nanofibrous mats for wound dressing application, the mechanical properties of PVA-Gly, PAN, and CS nanofibrous mats were evaluated through a tensile test. The test used a CTX texture analyzer (AMETEK Brookfield, US) with a 10 N load cell. The analyzer was equipped with handles designed for thin and delicate samples. Rectangular samples with 10 × 40 mm dimensions were securely placed during the test. The thickness of the nonwoven materials was measured with Kroeplin flat calipers for each sample and then averaged for further analysis. The crosshead speed was set at 0.5 mm/s. By analyzing the stress-strain curves obtained from the test, essential mechanical parameters such as Young's modulus, tensile strength, and elongation at break were determined. Each formulation was subjected to three repetitions, and the tests were performed on dry samples under ambient conditions.

Mucoadhesion Evaluation. The mucoadhesive properties of the nonwoven materials (PVA-Gly, PAN, CS) were assessed using a CTX texture analyzer equipped with a 1 kg load cell from AMETEK Brookfield, US. For testing, round samples of the nonwovens with a 10 mm diameter were affixed to a 10 mm diameter, 35 mm long cylinder probe using double-sided adhesive tape. Custom holders were used to secure freshly prepared filter sheets soaked in mucin. The testing procedure involved lowering the probe at a speed of 1 mm/s until the nonwoven made contact with the mucin disc, with a force of 0.05 N detected. After maintaining contact for 60 seconds with a constant force of 0.5 N, the probe was moved upwards at 1 mm/s to separate the sample from the mucin disc. A fresh mucin disc was used for each measurement. The mucoadhesive characteristics were determined by analyzing the maximum force required to detach the nonwoven from the mucin disc and the total work needed for the detachment process. The work of the mucoadhesion was quantified by calculating the area under the force vs. distance curve. Each type of nonwoven was subjected to three repetitions of the test under dry conditions.

Nanoplatform Behavior in Water Environment

Water Solubility Tests. Three circular samples of similar thickness with a diameter of 1.0 cm were cut out from PVA-Gly and CS mats and placed in separate vials containing 1 mL of deionized water. The samples were kept in the solution for up to one month and then were dried at room temperature, followed by (scanning electron microscopy) SEM imaging to observe the morphological changes.

Surface Wettability: Surface wettability was assessed by conducting contact angle measurements using the Data Physics OCA 15EC (Germany) instrument. Three water contact angle measurements were performed on each sample. The samples were positioned on a microscope glass slide, and a 2 µL water droplet with 1 µL/s dosing rate was applied to each sample at room temperature.

Degradation Study. About 10 mg of every sample, including PVA-Gly, PAN, and CS was carefully measured and then placed into the Eppendorf tubes. The samples were poured with 1 mL of PBS (pH=7.4) and put into the incubator. The temperature was maintained at 37 ºC during the whole process. The samples were completely dried out using the oven set to 50 ºC for 24 h at each predefined time point. Materials were weighted and poured with a fresh PBS portion.

Swelling Tests. Platform portions of 10 mg were precisely prepared and measured in terms of weight for each sample type (PVA-Gly, PAN, and CS). The samples were placed in Eppendorf tubes poured with 1 mL of PBS (pH=7.4) and placed into the incubator. The temperature was maintained at 37ºC during the whole process. The samples were collected at each predefined time point. The whole water was wiped out carefully from the material surface, and the samples were weighed. The medium was replaced with fresh PBS at each time point.

In Vitro **Drug Release Studies**. We investigated the release of various bioactive molecules (Ibuprofen, Ketoprofen, Dexketoprofen, Dexamethasone, Norfloxacin) placed in the core within CS fibers. In each case, a 5% mass ratio of the drugs relative to the polymer was used for the core preparation. To comprehensively examine the drug release mechanism from the CS structure, we additionally compared the release studies separately from the shell, the core, and the CS system. For this investigation, we selected Ibuprofen, which exhibited the highest release profile among all the examined drugs. The drug release studies were conducted as follows: approximately 10 mg of each material –CS, core, or shell were weighed and placed in the testing tubes. The samples were poured with 1 mL of PBS (pH = 7.4) and put into the incubator. The temperature was maintained at 37 ºC during the whole process. The medium was collected and replaced with fresh PBS at each predefined time point. The sample absorbance was measured using a UV-spectrometer (A Multiskan GO spectrophotometer, Thermo Scientific, USA) at the maximum wavelength absorbance of Ibuprofen (λ_{max} = 241 nm). The concentration was calculated using a calibration curve prepared from the Ibuprofen solutions of known concentration. The release of other drugs was conducted using the same principle by selecting the maximum wavelength absorbance for a specific compound.

In Vitro **Cell Studies**

Cell Culture. L929 murine fibroblast cells purchased from Sigma-Aldrich were cultured in DMEM (high glucose medium) supplemented with 10% FBS and 1% P/S at 37°C in 5% CO2 atmosphere. When the confluence of cells reached approximately ∼80%, the cells were collected using 0.05% EDTA-trypsin and centrifuged at 1200 rpm for 5 min. The fibrous mats ("sample") were sterilized by exposure to UV light (30 min cycle for each side). The cell suspension was diluted in the culture media to attain a seeding density of 10,000 cells per sample for the direct test or 5,000 cells per well for the indirect test.

Cell Seeding for Direct Tests. Collected cells were seeded on the top of CS-A, CS-G, CS-AG, and CS samples at a density of 10,000 cells/sample (diameter = 1.5 cm). The control condition was performed by seeding the same concentration of cells on tissue culture plates (TCP). The seeded samples were hydrated every 30 min with 30 µL of warm media for 4h. Thereafter, 1 mL of DMEM

media (supplemented with 10% FBS and 1% P/S) was added into each well with cell-seeded samples. The medium was changed every 2 days, and the culture took place over 7 days.

Cell Seeding for Indirect tests. To deeply examine the impact of the molecules released from samples on cell survival and proliferation, the indirect method using ISO 10993-12:2021 standard was evaluated. The sample extracts from selected CS-A and CS mats were prepared as follows: electrospun mats were cut to match the 6 cm^2/mL standard extraction ratio. The samples were sterilized under UV (2x30 min on both sides) and placed in media (DMEM+FBS+PS) for 24 hours at 37°C with a 5% CO_2 atmosphere. Then, the extracts were collected and additionally sterilized using a 0.2μm filter. L929 fibroblast cells were seeded in the 96 well-plate at a density of 5,000 cells per well. The media was changed using prepared extracts (Extr_CS-A and Extr_CS) or pure media (DMEM).

Cell Proliferation for Direct and Indirect Tests. To obtain a quantitative assessment of the cells' viability, the proliferation was measured with PrestoBlue assay on 1, 3, and 7 days of cell culture for both direct and indirect tests. The samples and controls (five replicates per group) were treated with a solution of 10% (v/v) PrestoBlue reagent in culture medium and incubated for 2 h at 37 °C and 5% CO_2. After that, triplicates of each 100 μL aliquots of the PrestoBlue solution were transferred to a 96-well plate and analyzed at excitation 530 nm and emission at 620 nm by using a fluorometer plate reader (Fluoroskan Ascent TM Microplate Fluorometer, Thermo Scientific, USA).

Cell Morphology for Direct Tests. The cell morphology seeded on the samples was examined using SEM on triplicate samples after 3 days of cell culture. The samples were first fixed in 3% ice-cold GTA for 3 hours. Following three washes in DI water, the samples were dehydrated by immersing them for 15 minutes in solutions with increasing ethanol concentrations: 50%, 70%, 90%, and finally, 100%. Subsequently, HMDS was introduced to the constructs, and the samples were left to dry overnight under a fume hood. Finally, the samples were coated with a thin layer of gold using sputter coating and then imaged using SEM.

Live/Dead Essay for Indirect Tests. To obtain a qualitative assessment of the cell's viability treated with extracts, a Live/Dead assay was performed on day 7 of culture to detect any potential cytotoxicity of the materials. The cells were washed with PBS and incubated for 10 min in a dye solution: 0.5 μL calcein (staining live cells green) with 2 μL ethidium homodimer (staining dead cells red) dissolved in 1 mL sterile PBS. Following washing the cell samples three times with PBS, a confocal microscope (TCS SP5 X, Leica, Germany) visualization was performed.

Confocal Imaging of Cell Cytoskeleton for Indirect Tests. For immunofluorescence staining, cells treated with extracts were initially washed with PBS and fixed in 4% paraformaldehyde for 15 minutes at room temperature. Subsequently, after washing, the samples underwent incubation in a 0.3% (v/v) Triton X-100 solution for 15 minutes, followed by incubation in 1% (w/v) BSA with 0.1% Triton X-100 for 1 hour. Following another round of washing, the samples were incubated with 1% BSA + 0.1% Triton X-100 + 1:40 Alexa Fluor 488 Phalloidin for 1 hour in the dark. After a final wash, the samples were stained with a solution of 1:500 DAPI in PBS for 10 minutes. Post-staining, samples were washed, and the cell cytoskeleton and nuclei were visualized using a confocal microscope.

Ex vivo **Studies on Human EpiDerm™**

EpiDerm™ (EPI-200), reconstructed human epidermal tissues utilize semipermeable inserts for the cultivation of human epidermal keratinocytes at the air-liquid interface. On receipt, tissues were promptly placed in 6-well plates containing 0.9 mL of medium provided by the manufacturer.

Before chemical substance testing, tissues were conditioned overnight in a humidified incubator under standard conditions (37°C, 5% CO_2) to ensure removal from transport agarose and proper adaptation. To prepare extracts from the polymers investigated to assess their impact on the epidermis, a methodology compliant with ISO 10993-12:2021 was used. Samples with a thickness of <0.5 mm were extracted in a ratio of 6 cm^2/mL in a 0.9% NaCl solution for 24 hours at a temperature of 37°C with continuous stirring and shaking to ensure the extraction process was completed at the end of the EpiDerm^{TM} preincubation period.

The *in vitro* irritation test was conducted following the protocol outlined by MatTek Corporation and in accordance with the guidelines of the International Standards Organization (ISO/TC 194 WG 8 Irritation and Skin Sensitization). The samples were divided into four groups. Each was then treated with 100 μL of the test substances: Negative control - Dulbecco's phosphate buffered saline, positive control - 1% solution of sodium dodecyl sulfate, and the experimental groups were treated with extracts from polymer CS and CS-A. After substance treatment, the tissues were incubated for 18 hours under standard controlled conditions. After incubation, a viability test and histological examination were performed immediately to assess tissue response. The collected fluids after incubation were used for lactate dehydrogenase (LDH) activity tests.

Tissue Viability and Cytotoxicity of Extracts. Evaluation of tissue viability under the influence of tested substances was carried out using the MTT enzyme reduction assay, following the manufacturer's recommendations and the ISO 10993-10:2021 standard guidelines pertinent to this method. For the assay, Epiderm^{TM} inserts were placed in a 24-well plate and loaded with 300 μL of a 1 mg/mL solution of MTT, prepared in the appropriate medium provided with the tissues. Subsequently, the samples were incubated for 3 hours at 37 °C. Upon completion of incubation, tissues were transferred to another set of 24-well plates containing 2.0 mL of isopropyl alcohol, and the absorbance of the samples was read at 570 nm using a spectrophotometer.

Additionally, to assess cell membrane permeability, lactate dehydrogenase (LDH) activity in the cell media was measured using the CytoScan LDH Cytotoxicity Assay kit. After the transfer of 50 μL of each sample medium to a 96-well plate, a reaction mixture was added and incubated for 30 minutes at room temperature. After the reaction was quenched with a stopping solution, the absorbance was read at 490 and 680 nm.

In both assays, an Infnite® 200 PRO microplate reader and i-controlTM software (Tecan Group Ltd., Männedorf, Switzerland), were used to measure absorbance and the percentage of control was determined using the equation: % control = OD (treated tissue) / OD (negative control tissue) x 100.

Histological Evaluation. The preparation of the tissue for histological characterization involved first subjecting them to fixation by overnight incubation in 4% formalin at 4 °C. Subsequently, for further tissue processing, the epidermis was dehydrated using an alcohol gradient. This process entailed sequential immersion of tissues in 30% ethanol solution, followed by 50% ethanol for 2 hours each, and then in 70% ethanol overnight. The samples were then immersed in two rounds of immersion of 95% ethanol for 3 hours each, followed by two rounds of 100% ethanol. Following tissue fixation and dehydration, sectioning was performed according to the experimental protocol to obtain suitable fragments for analysis. Subsequently, standard hematoxylin and eosin (H&E) staining was carried out to highlight the morphology and tissue structure, enabling their precise characterization.

***In Vitro* Assessment of Antibacterial Activities**

Bacteria culture. *Staphylococcus aureus* (*S. Aureus*) ATCC 25923 was cultured on lysogeny broth (LB) agar and isolated using the streak plate method. One isolated colony was inoculated into fresh LB broth (3 mL) and incubated at 36°C overnight in an orbital shaker for testing.

Qualitative Antibacterial Activity Studies. Circular samples of CS, CS-A, and CS-NOR measuring 9 mm underwent sterilization under ultraviolet light for a total of 1 hour on both sides. An overnight culture of *S. Aureus* bacteria was diluted in sterile PBS to 10^6 colony-forming units (CFU)/mL. A transferring loop was used to evenly disperse 100 µL of the resulting diluted bacteria suspensions on the surface of the agar medium slope. Next, the CS, CS-A, and CS-NOR were placed on them. The control sample consisted of plates solely inoculated with bacteria (CTRL). The samples were incubated overnight at 36 °C for macroscopic visualization.

Quantitative Antibacterial Activity Evaluation. Circular samples of CS, CS-A, and CS-NOR measuring 6 mm in diameter underwent sterilization under ultraviolet light for a total of 1 hour on both sides and glued on the bottom of the 96 well plates. The *S. Aureus* colony with 10^6 dilutions was added to the samples in the volume of 100 µL each sample. Pure bacterial suspension serves as a positive control. The prepared samples were incubated for 3h at 37 °C, and then solutions were transferred to a new 96-well plate and serially diluted before plating on LB agar plates. Bacterial colonies were counted after overnight incubation at 36 °C to assess bacterial survival.

Skin Patch *In Vivo* Human Studies

Volunteers representing diverse geographic locations and skin types (5 Polish, 2 Italians, and 1 Iranian) aged 25-42 took part in the evaluation of patches. One patient suffers from atopic dermatitis (eczema). Commercial cotton-wool gauze (Group 1), commercial cotton-wool gauze soaked with fermented argan oil (Group 2), CS (Group 3), CS-A (Group 4) was chosen to evaluate patches as skin hydration patches. Prior to testing, skin hydration was assessed using a digital skin condition analyzer (Minimo, USA). The patches were cut into rectangular shapes (2×3 cm) and applied to the forearm skin. Medical paper tape (3M, USA) was used to secure the patches, and the tape was applied to all edges of the samples. Group 0 served as the negative control group, with the skin left untreated without the application of any patch. The patches were worn during the day under regular activity conditions without outerwear. The skin hydrations were measured at each site before application of the patches (time 0 – control), after 3 h, and after 6 hours, and then the patches were removed. Afterward, a macroscopic assessment of skin irritation and potential allergic reactions was conducted. Five skin hydration measurements were taken at each measurement for each of the five groups to determine the average and standard deviation. It is important to note that this study had statistical limitations, as it involved only eight volunteers. However, the objective was to demonstrate the application principle of the manufactured patches. The testing of patches on human skin was conducted in accordance with ethical considerations for human testing of cosmetic products, as outlined by the EU Council Directive (76/768/EEC) and the World Medical Association Declaration of Helsinki (1964-1975-1983-1989-1996). Written and signed agreements have been obtained from each volunteer for the experiments.

Statistical analysis

The data underwent statistical analysis using a one-way ANOVA followed by Tukey's multiple pairwise comparisons test calculated by OriginPro software. Significance was set at the 0.05 level. For each measurement, 5 samples per group were tested, unless otherwise noted in the study.

ASSOCIATED CONTENT

The Supporting Information is available free of charge at…
Figure S1. Schematic illustration of eco-friendly Gly crosslinking of polyvinyl alcohol. Figure S2. The Influence of Gly on Oil Solubility and Nanoplatform Behavior in an Aquatic Environment. Figure S3. Solubility assessment of PVA-Gly and CS nanofibers in a water environment over 1 month by scanning electron microscopy images. Figure S4. Physico-chemical characterization of PVA fibers without crosslinking and Gly solution. Figure S5. Application of the different patches on the finger illustrating the material's strong adhesion during bending at 0°, 45°, and 90° positions. Figure S6. Characterization of CS nanofibers with ferment oils: argan oil (CS-A), green tea oil (CS-G), a combination of argan and green tea oils (CS-AG), and without oils (CS).

AUTHOR INFORMATION

*Corresponding Author
Filippo Pierini - Department of Biosystems and Soft Matter, Institute of Fundamental Technological Research, Polish Academy of Sciences, Warsaw 02-106, Poland; orcid.org/0000-0002-6526-4141; Email: fpierini@ippt.pan.pl

Authors
Alicja Kosik-Kozioł - Department of Biosystems and Soft Matter, Institute of Fundamental Technological Research, Polish Academy of Sciences, Warsaw 02-106, Poland; orcid.org/0000-0002-2607-7271; Email: akoziol@ippt.pan.pl
Paweł Nakielski - Department of Biosystems and Soft Matter, Institute of Fundamental Technological Research, Polish Academy of Sciences, Warsaw 02-106, Poland; orcid.org/0000-0001-6194-701X; Email: pnakiel@ippt.pan.pl
Daniel Rybak - Department of Biosystems and Soft Matter, Institute of Fundamental Technological Research, Polish Academy of Sciences, Warsaw 02-106, Poland; orcid.org/0000-0001-7319-8810; Email: drybak@ippt.pan.pl
Wiktoria Fraczek - Department of Nanobiotechnology, Institute of Biology, Warsaw University of Life Sciences, Warsaw, Poland; orcid.org/0000-0001-9328-3422; Email: wiktoria_fraczek@sggw.edu.pl
Chiara Rinoldi - Department of Biosystems and Soft Matter, Institute of Fundamental Technological Research, Polish Academy of Sciences, Warsaw 02-106, Poland; orcid.org/0000-0002-4028-375X; Email: crinoldi@ippt.pan.pl
Massimiliano Lanzi - Department of Industrial Chemistry "Toso Montanari", Alma Mater Studiorum University of Bologna, Bologna 40136, Italy; orcid.org/0000-0002-2466-2813; Email: massimiliano.lanzi@unibo.it
Marta Grodzik - Department of Nanobiotechnology, Institute of Biology, Warsaw University of Life Sciences, Warsaw, Poland; orcid.org/0000-0001-5359-1885; Email: marta_grodzik@sggw.edu.pl

Author Contributions

AKK designed the experiments, performed *in vitro* cell study, *in vivo* application tests, *in vitro* bacteria study, and physico-chemical experiments, analyzed the data, wrote the manuscript, prepared graphical illustrations, PN performed the mechanical experiments, edited the manuscript, participated in patch applications visualizations, DR performed the swelling tests, drugs release and degration tests, WF performed *ex vivo* study, CR participated in *in vitro* bacteria study, ML performed TGA study, MG performed *ex vivo* study, FP edited the manuscript, designed the experiments and supervised the project. All the authors proofread the manuscript.

Notes

The authors declare no competing financial interest. Patients participating in *in vivo* study signed an agreement allowing the use, processing of biological patches, and disseminate of data for scientific purposes.

ABBREVIATIONS

For clarity of the article, we used the following nomenclature throughout the text: PVA-Gly (for the shell, green-crosslinking method), PAN (core), CS (core-shell), CS-A (core-shell loaded with argan oil), CS-G (core-shell loaded with green tea oil), CS-AG (core-shell loaded with argan and green tea oils), Extr_CS (extracts from the CS mats), Extr_CS-A (extracts from the CS-A mats), CS-NOR (core-shell loaded with antibiotic Norfloxacin).

REFERENCES

(1)   Sidbury, R.; Davis, D. M.; Cohen, D. E.; Cordoro, K. M.; Berger, T. G.; Bergman, J. N.; Chamlin, S. L.; Cooper, K. D.; Feldman, S. R.; Hanifin, J. M.; Krol, A.; Margolis, D. J.; Paller, A. S.; Schwarzenberger, K.; Silverman, R. A.; Simpson, E. L.; Tom, W. L.; Williams, H. C.; Elmets, C. A.; Block, J.; Harrod, C. G.; Begolka, W. S.; Eichenfield, L. F.; American Academy of Dermatology. Guidelines of Care for the Management of Atopic Dermatitis: Section 3. Management and Treatment with Phototherapy and Systemic Agents. *J. Am. Acad. Dermatol.* **2014**, *71* (2), 327–349. DOI: 10.1016/j.jaad.2014.03.030.

(2)   Shadi, T. Z.; Talal, A. Z. A Review of Four Common Medicinal Plants Used to Treat Eczema. *J. Med. Plants Res.* **2015**, *9* (24), 702–711. DOI: 10.5897/JMPR2015.5831.

(3)   Campos, E. V. R.; Proença, P. L. F.; Costa, T. G. da; de Lima, R.; Hedtrich, S.; Fraceto, L. F.; de Araujo, D. R. Hydrogels Containing Budesonide-Loaded Nanoparticles to Facilitate Percutaneous Absorption for Atopic Dermatitis Treatment Applications. *ACS Appl. Polym. Mater.* **2021**, *3* (9), 4436–4449. DOI: 10.1021/acsapm.1c00021.

(4)   Nygaard, U.; Deleuran, M.; Vestergaard, C. Emerging Treatment Options in Atopic Dermatitis: Topical Therapies. *Dermatology (Basel)* **2017**, *233* (5), 333–343. DOI: 10.1159/000484407.

(5)   Krysiak, Z. J.; Knapczyk-Korczak, J.; Maniak, G.; Stachewicz, U. Moisturizing Effect of Skin Patches with Hydrophobic and Hydrophilic Electrospun Fibers for Atopic Dermatitis. *Colloids Surf. B Biointerfaces* **2021**, *199*, 111554. DOI: 10.1016/j.colsurfb.2020.111554.

(6)   Sethuram, L.; Thomas, J. Therapeutic Applications of Electrospun Nanofibers Impregnated with Various Biological Macromolecules for Effective Wound Healing Strategy - A Review. *Biomed. Pharmacother.* **2023**, *157*, 113996. DOI: 10.1016/j.biopha.2022.113996.

(7)   Mirbagheri, M. S.; Akhavan-Mahdavi, S.; Hasan, A.; Kharazmi, M. S.; Jafari, S. M. Chitosan-Based Electrospun Nanofibers for Diabetic Foot Ulcer Management; Recent Advances. *Carbohydr. Polym.* **2023**, *313*, 120512. DOI: 10.1016/j.carbpol.2022.120512.

(8)   Anaya Mancipe, J. M.; Boldrini Pereira, L. C.; de Miranda Borchio, P. G.; Dias, M. L.; da Silva Moreira Thiré, R. M. Novel Polycaprolactone (PCL)-Type I Collagen Core-Shell Electrospun Nanofibers for Wound Healing Applications. *J. Biomed. Mater. Res. Part B Appl. Biomater.* **2023**, *111* (2), 366–381. DOI: 10.1002/jbm.b.35156.

(9)   D'souza, O. J.; Gasti, T.; Hiremani, V. D.; Pinto, J. P.; Contractor, S. S.; Shettar, A. K.; Olivia, D.; Arakera, S. B.; Masti, S. P.; Chougale, R. B. Basella Alba Stem Extract Integrated Poly (Vinyl Alcohol)/Chitosan Composite Films: A Promising Bio-Material for Wound Healing. *Int. J. Biol. Macromol.* **2023**, *225*, 673–686. DOI: 10.1016/j.ijbiomac.2022.11.130.

(10)   Parın, F. N. A Green Approach to the Development of Novel Antibacterial Cinnamon Oil Loaded-PVA/Egg White Foams via Pickering Emulsions. *J. Porous Mater.* **2023**, *30* (4), 1233–1243. DOI: 10.1007/s10934-022-01417-9.

(11)   Lan, Z.; Kar, R.; Chwatko, M.; Shoga, E.; Cosgriff-Hernandez, E. High Porosity PEG-Based Hydrogel Foams with Self-Tuning Moisture Balance as Chronic Wound Dressings. *J. Biomed. Mater. Res. A* **2023**, *111* (4), 465–477. DOI: 10.1002/jbm.a.37498.

(12)   Jia, B.; Li, G.; Cao, E.; Luo, J.; Zhao, X.; Huang, H. Recent Progress of Antibacterial Hydrogels in Wound Dressings. *Mater. Today Bio* **2023**, *19*, 100582. DOI: 10.1016/j.mtbio.2023.100582.

(13)   Wang, W.; Ummartyotin, S.; Narain, R. Advances and Challenges on Hydrogels for Wound Dressing. *Curr. Opin. Biomed. Eng* **2023**, *26*, 100443. DOI: 10.1016/j.cobme.2022.100443.

(14)   Barjasteh, M.; Dehnavi, S. M.; Ahmadi Seyedkhani, S.; Rahnamaee, S. Y.; Golizadeh, M. Improved Biological Activities of Dual Nanofibrous Chitosan/Bacterial Cellulose Wound Dressing by a Novel Silver-Based Metal-Organic Framework. *Surfaces and Interfaces* **2023**, *36*, 102631. DOI: 10.1016/j.surfin.2023.102631.

(15)   Cullen, B.; Gefen, A. The Biological and Physiological Impact of the Performance of Wound Dressings. *Int. Wound J.* **2023**, *20* (4), 1292–1303. DOI: 10.1111/iwj.13960.

(16)   Shao, Z.; Yin, T.; Jiang, J.; He, Y.; Xiang, T.; Zhou, S. Wound Microenvironment Self-Adaptive Hydrogel with Efficient Angiogenesis for Promoting Diabetic Wound Healing. *Bioact. Mater.* **2023**, *20*, 561–573. DOI: 10.1016/j.bioactmat.2022.06.018.

(17)   Haghighat Bayan, M. A.; Dias, Y. J.; Rinoldi, C.; Nakielski, P.; Rybak, D.; Truong, Y. B.; Yarin, A. L.; Pierini, F. Near-infrared Light Activated Core-shell Electrospun Nanofibers Decorated with Photoactive Plasmonic Nanoparticles for On-demand Smart Drug Delivery Applications. *J. Polym. Sci.* **2023**, 1–13. DOI: 10.1002/pol.20220747.

(18)   Parın, F. N.; Aydemir, Ç. İ.; Taner, G.; Yıldırım, K. Co-Electrospun-Electrosprayed PVA/Folic Acid Nanofibers for Transdermal Drug Delivery: Preparation, Characterization, and in Vitro Cytocompatibility. *Journal of Industrial Textiles* **2021**, 152808372199718. DOI: 10.1177/1528083721997185.

(19)   Gupta, S.; Webster, T. J.; Sinha, A. Evolution of PVA Gels Prepared without Crosslinking Agents as a Cell Adhesive Surface. *J. Mater. Sci. Mater. Med.* **2011**, *22* (7), 1763–1772. DOI: 10.1007/s10856-011-4343-2.

(20)   Zakrzewska, A.; Zargarian, S. S.; Rinoldi, C.; Gradys, A.; Jarząbek, D.; Zanoni, M.; Gualandi, C.; Lanzi, M.; Pierini, F. Electrospun Poly(Vinyl Alcohol)-Based Conductive Semi-Interpenetrating Polymer Network Fibrous Hydrogel: A Toolbox for Optimal Cross-Linking. *ACS Mater. Au* **2023**. DOI: 10.1021/acsmaterialsau.3c00025.

(21)   Han, X.; Huo, P.; Ding, Z.; Kumar, P.; Liu, B. Preparation of Lutein-Loaded PVA/Sodium Alginate Nanofibers and Investigation of Its Release Behavior. *Pharmaceutics* **2019**, *11* (9). DOI: 10.3390/pharmaceutics11090449.

(22)   Fatih Isik, A.; San Keskin, N. O.; Ulcay, Y. Synthesis and in Vitro Antimicrobial Characterization of Boron-PVA Electrospun Nanofibers. *The Journal of The Textile Institute* **2018**, *110* (4), 1–6. DOI: 10.1080/00405000.2018.1496989.

(23)   Nagakawa, Y.; Kato, M.; Suye, S.-I.; Fujita, S. Fabrication of Tough, Anisotropic, Chemical-Crosslinker-Free Poly(Vinyl Alcohol) Nanofibrous Cryogels via Electrospinning. *RSC Adv.* **2020**, *10* (62), 38045–38054. DOI: 10.1039/d0ra07322a.

(24)   Peng, S.; Liu, S.; Sun, Y.; Xiang, N.; Jiang, X.; Hou, L. Facile Preparation and Characterization of Poly(Vinyl Alcohol)-NaCl-Glycerol Supramolecular Hydrogel Electrolyte. *Eur. Polym. J.* **2018**, *106*, 206–213. DOI: 10.1016/j.eurpolymj.2018.07.024.

(25)   Shi, S.; Peng, X.; Liu, T.; Chen, Y.-N.; He, C.; Wang, H. Facile Preparation of Hydrogen-Bonded Supramolecular Polyvinyl Alcohol-Glycerol Gels with Excellent Thermoplasticity and Mechanical Properties. *Polymer* **2017**, *111*, 168–176. DOI: 10.1016/j.polymer.2017.01.051.

(26)   Huang, C.; Xu, X.; Fu, J.; Yu, D.-G.; Liu, Y. Recent Progress in Electrospun Polyacrylonitrile Nanofiber-Based Wound Dressing. *Polymers (Basel)* **2022**, *14* (16). DOI: 10.3390/polym14163266.

(27)   Hashmi, M.; Ullah, S.; Kim, I. S. Copper Oxide (CuO) Loaded Polyacrylonitrile (PAN) Nanofiber Membranes for Antimicrobial Breath Mask Applications. *Current Research in Biotechnology* **2019**, *1*, 1–10. DOI: 10.1016/j.crbiot.2019.07.001.

(28)   Park, M. J.; Gonzales, R. R.; Abdel-Wahab, A.; Phuntsho, S.; Shon, H. K. Hydrophilic Polyvinyl Alcohol Coating on Hydrophobic Electrospun Nanofiber Membrane for High Performance Thin Film Composite Forward Osmosis Membrane. *Desalination* **2018**, *426*, 50–59. DOI: 10.1016/j.desal.2017.10.042.

(29)   Rybak, D.; Rinoldi, C.; Nakielski, P.; Du, J.; Haghighat Bayan, M. A.; Zargarian, S. S.; Pruchniewski, M.; Li, X.; Strojny-Cieślak, B.; Ding, B.; Pierini, F. Injectable and Self-Healable Nano-Architectured Hydrogel for NIR-Light Responsive Chemo- and Photothermal Bacterial Eradication. *J. Mater. Chem. B Mater. Biol. Med.* **2024**, *12* (7), 1905–1925. DOI: 10.1039/d3tb02693k.

(30)   Ziai, Y.; Petronella, F.; Rinoldi, C.; Nakielski, P.; Zakrzewska, A.; Kowalewski, T. A.; Augustyniak, W.; Li, X.; Calogero, A.; Sabała, I.; Ding, B.; De Sio, L.; Pierini, F. Chameleon-Inspired Multifunctional Plasmonic Nanoplatforms for Biosensing Applications. *NPG Asia Mater.* **2022**, *14* (1), 18. DOI: 10.1038/s41427-022-00365-9.

(31)   Nakielski, P.; Pawłowska, S.; Rinoldi, C.; Ziai, Y.; De Sio, L.; Urbanek, O.; Zembrzycki, K.; Pruchniewski, M.; Lanzi, M.; Salatelli, E.; Calogero, A.; Kowalewski, T. A.; Yarin, A. L.; Pierini, F. Multifunctional Platform Based on Electrospun Nanofibers and Plasmonic Hydrogel: A Smart Nanostructured Pillow for Near-Infrared Light-Driven Biomedical Applications. *ACS Appl. Mater. Interfaces* **2020**, *12* (49), 54328–54342. DOI: 10.1021/acsami.0c13266.

(32)   Halcon, L.; Milkus, K. Staphylococcus Aureus and Wounds: A Review of Tea Tree Oil as a Promising Antimicrobial. *Am. J. Infect. Control* **2004**, *32* (7), 402–408. DOI: 10.1016/j.ajic.2003.12.008.

(33)   Tsoureli-Nikita, E.; Hercogova, J.; Lotti, T.; Menchini, G. Evaluation of Dietary Intake of Vitamin E in the Treatment of Atopic Dermatitis: A Study of the Clinical Course and

Evaluation of the Immunoglobulin E Serum Levels. *Int. J. Dermatol.* **2002**, *41* (3), 146–150. DOI: 10.1046/j.1365-4362.2002.01423.x.

(34)   Avsar, U.; Halici, Z.; Akpinar, E.; Yayla, M.; Avsar, U.; Harun, U.; Harun, U.; Hasan Tarik, A.; Bayraktutan, Z. The Effects of Argan Oil in Second-Degree Burn Wound Healing in Rats. *Ostomy Wound Manage.* **2016**, *62* (3), 26–34.

(35)   Alonso-López, O.; López-Ibáñez, S.; Beiras, R. Assessment of Toxicity and Biodegradability of Poly(Vinyl Alcohol)-Based Materials in Marine Water. *Polymers (Basel)* **2021**, *13* (21). DOI: 10.3390/polym13213742.

(36)   Walser, J.; Ferguson, S. J. Oriented Nanofibrous Membranes for Tissue Engineering Applications: Electrospinning with Secondary Field Control. *J. Mech. Behav. Biomed. Mater.* **2016**, *58*, 188–198. DOI: 10.1016/j.jmbbm.2015.06.027.

(37)   Li, J.; Su, S.; Zhou, L.; Kundrát, V.; Abbot, A. M.; Mushtaq, F.; Ouyang, D.; James, D.; Roberts, D.; Ye, H. Carbon Nanowalls Grown by Microwave Plasma Enhanced Chemical Vapor Deposition during the Carbonization of Polyacrylonitrile Fibers. *J. Appl. Phys.* **2013**, *113* (2). DOI: 10.1063/1.4774218.

(38)   Kataoka, Y.; Kitadai, N.; Hisatomi, O.; Nakashima, S. Nature of Hydrogen Bonding of Water Molecules in Aqueous Solutions of Glycerol by Attenuated Total Reflection (ATR) Infrared Spectroscopy. *Appl. Spectrosc.* **2011**, *65* (4), 436–441. DOI: 10.1366/10-06183.

(39)   Kharazmi, A.; Faraji, N.; Mat Hussin, R.; Saion, E.; Yunus, W. M. M.; Behzad, K. Structural, Optical, Opto-Thermal and Thermal Properties of ZnS-PVA Nanofluids Synthesized through a Radiolytic Approach. *Beilstein J. Nanotechnol.* **2015**, *6*, 529–536. DOI: 10.3762/bjnano.6.55.

(40)   Pawłowska, S.; Rinoldi, C.; Nakielski, P.; Ziai, Y.; Urbanek, O.; Li, X.; Kowalewski, T. A.; Ding, B.; Pierini, F. Ultraviolet Light-assisted Electrospinning of Core–Shell Fully Cross-linked p(Nipaam- *Co* -nipmaam) Hydrogel-based Nanofibers for Thermally Induced Drug Delivery Self-regulation. *Adv. Mater. Interfaces* **2020**, *7* (12), 2000247. DOI: 10.1002/admi.202000247.

(41)   Tang, C.-M.; Tian, Y.-H.; Hsu, S.-H. Poly(Vinyl Alcohol) Nanocomposites Reinforced with Bamboo Charcoal Nanoparticles: Mineralization Behavior and Characterization. *Materials (Basel)* **2015**, *8* (8), 4895–4911. DOI: 10.3390/ma8084895.

(42)   Gupta, S.; Pramanik, A. K.; Kailath, A.; Mishra, T.; Guha, A.; Nayar, S.; Sinha, A. Composition Dependent Structural Modulations in Transparent Poly(Vinyl Alcohol) Hydrogels. *Colloids Surf. B Biointerfaces* **2009**, *74* (1), 186–190. DOI: 10.1016/j.colsurfb.2009.07.015.

(43)   Alakanandana, A.; Subrahmanyam, A. R.; Siva Kumar, J. Structural and Electrical Conductivity Studies of Pure PVA and PVA Doped with Succinic Acid Polymer

Electrolyte System. *Materials Today: Proceedings* **2016**, *3* (10), 3680–3688. DOI: 10.1016/j.matpr.2016.11.013.

(44)   Saud, P. S.; Ghouri, Z. K.; Pant, B.; An, T.; Lee, J. H.; Park, M.; Kim, H.-Y. Photocatalytic Degradation and Antibacterial Investigation of Nano Synthesized Ag_3VO_4 Particles @PAN Nanofibers. *Carbon letters* **2016**, *18*, 30–36. DOI: 10.5714/CL.2016.18.030.

(45)   Jawadi, Z.; Yang, C.; Haidar, Z. S.; Santa Maria, P. L.; Massa, S. Bio-Inspired Muco-Adhesive Polymers for Drug Delivery Applications. *Polymers (Basel)* **2022**, *14* (24). DOI: 10.3390/polym14245459.

(46)   Cheng, X.; Yang, Y.; Liao, Z.; Yi, Q.; Zhou, Y.; Dai, X.; Liu, Y.; Liu, O. Drug-Loaded Mucoadhesive Microneedle Patch for the Treatment of Oral Submucous Fibrosis. *Front. Bioeng. Biotechnol.* **2023**, *11*, 1251583. DOI: 10.3389/fbioe.2023.1251583.

(47)   Lee, J.; Kim, D.; Bang, S.; Park, S. Drug-Loaded Mucoadhesive Patch with Active Delivery and Controlled Releasing Ability. *Advanced Intelligent Systems* **2022**, 2100203. DOI: 10.1002/aisy.202100203.

(48)   Delrio, F. W.; de Boer, M. P.; Knapp, J. A.; David Reedy, E.; Clews, P. J.; Dunn, M. L. The Role of van Der Waals Forces in Adhesion of Micromachined Surfaces. *Nat. Mater.* **2005**, *4* (8), 629–634. DOI: 10.1038/nmat1431.

(49)   Chen, S.; Zhang, K.; Li, Z.; Wu, Y.; Zhu, B.; Zhu, J. Hydrogen-Bonded Supramolecular Adhesives: Synthesis, Responsiveness, and Application. *Supramolecular Materials* **2023**, *2*, 100032. DOI: 10.1016/j.supmat.2023.100032.

(50)   Raos, G.; Zappone, B. Polymer Adhesion: Seeking New Solutions for an Old Problem. *Macromolecules* **2021**, *54* (23), 10617–10644. DOI: 10.1021/acs.macromol.1c01182.

(51)   Kusumaatmaja, A.; Nur, W.; Chotimah, C.; Triyana, K. Hydrophilic/Hydrophobic Property Changes on Polyacrylonitrile/Cellulose Acetate Nanofiber Membrane. *MSF* **2020**, *990*, 215–219. DOI: 10.4028/www.scientific.net/MSF.990.215.

(52)   Jung, B. Preparation of Hydrophilic Polyacrylonitrile Blend Membranes for Ultrafiltration. *J. Memb. Sci.* **2004**, *229* (1–2), 129–136. DOI: 10.1016/j.memsci.2003.10.020.

(53)   Liu, H.; Hsieh, Y. Preparation of Water-absorbing Polyacrylonitrile Nanofibrous Membrane. *Macromol. Rapid Commun.* **2006**, *27* (2), 142–145. DOI: 10.1002/marc.200500691.

(54)   Wang, S.; Pang, M.; Wen, Z. The Structure and Property of Polyacrylonitrile-Based Microfiltration Membranes for Oil-Water Emulsion Separation. *Journal of Industrial Textiles* **2022**, *51* (5_suppl), 8788S-8803S. DOI: 10.1177/15280837221107164.

(55) Oranje, A. P.; Devillers, A. C. A.; Kunz, B.; Jones, S. L.; DeRaeve, L.; Van Gysel, D.; de Waard-van der Spek, F. B.; Grimalt, R.; Torrelo, A.; Stevens, J.; Harper, J. Treatment of Patients with Atopic Dermatitis Using Wet-Wrap Dressings with Diluted Steroids and/or Emollients. An Expert Panel's Opinion and Review of the Literature. *J. Eur. Acad. Dermatol. Venereol.* **2006**, *20* (10), 1277–1286. DOI: 10.1111/j.1468-3083.2006.01790.x.

(56) Nowicki, R.; Trzeciak, M.; Wilkowska, A.; Sokołowska-Wojdyło, M.; Ługowska-Umer, H.; Barańska-Rybak, W.; Kaczmarski, M.; Kowalewski, C.; Kruszewski, J.; Maj, J.; Silny, W.; Śpiewak, R.; Petranyuk, A. Atopic Dermatitis: Current Treatment Guidelines. Statement of the Experts of the Dermatological Section, Polish Society of Allergology, and the Allergology Section, Polish Society of Dermatology. *Postepy Dermatol. Alergol.* **2015**, *32* (4), 239–249. DOI: 10.5114/pdia.2015.53319.

(57) González-López, G.; Ceballos-Rodríguez, R. M.; González-López, J. J.; Feito Rodríguez, M.; Herranz-Pinto, P. Efficacy and Safety of Wet Wrap Therapy for Patients with Atopic Dermatitis: A Systematic Review and Meta-Analysis. *Br. J. Dermatol.* **2017**, *177* (3), 688–695. DOI: 10.1111/bjd.15165.

(58) Devillers, A. C. A.; Oranje, A. P. Wet-Wrap Treatment in Children with Atopic Dermatitis: A Practical Guideline. *Pediatr. Dermatol.* **2012**, *29* (1), 24–27. DOI: 10.1111/j.1525-1470.2011.01691.x.

(59) Li, L.; Hao, R.; Qin, J.; Song, J.; Chen, X.; Rao, F.; Zhai, J.; Zhao, Y.; Zhang, L.; Xue, J. Electrospun Fibers Control Drug Delivery for Tissue Regeneration and Cancer Therapy. *Adv. Fiber Mater.* **2022**, *4* (6), 1375–1413. DOI: 10.1007/s42765-022-00198-9.

(60) Zielińska-Górska, M.; Sawosz, E.; Sosnowska, M.; Hotowy, A.; Grodzik, M.; Górski, K.; Strojny-Cieślak, B.; Wierzbicki, M.; Chwalibog, A. Molecular Biocompatibility of a Silver Nanoparticle Complex with Graphene Oxide to Human Skin in a 3D Epidermis In Vitro Model. *Pharmaceutics* **2022**, *14* (7). DOI: 10.3390/pharmaceutics14071398.

(61) Fraczek, W.; Kregielewski, K.; Wierzbicki, M.; Krzeminski, P.; Zawadzka, K.; Szczepaniak, J.; Grodzik, M. A Comprehensive Assessment of the Biocompatibility and Safety of Diamond Nanoparticles on Reconstructed Human Epidermis. *Materials (Basel)* **2023**, *16* (16). DOI: 10.3390/ma16165600.

(62) Kitisin, T.; Muangkaew, W.; Thitipramote, N.; Pudgerd, A.; Sukphopetch, P. The Study of Tryptophol Containing Emulgel on Fungal Reduction and Skin Irritation. *Sci. Rep.* **2023**, *13* (1), 18881. DOI: 10.1038/s41598-023-46121-z.

(63) Mizumachi, H.; Suzuki, S.; Sakuma, M.; Natsui, M.; Imai, N.; Miyazawa, M. Reconstructed Human Epidermis-Based Testing Strategy of Skin Sensitization Potential and Potency Classification Using Epidermal Sensitization Assay and in Silico Data. *J. Appl. Toxicol.* **2024**, *44* (3), 415–427. DOI: 10.1002/jat.4551.

(64)   Kandarova, H.; Willoughby, J. A.; De Jong, W. H.; Letasiova, S.; Milasova, T.; Bachelor, M. A.; Breyfogle, B.; Handa, Y.; De la Fonteyne, L.; Coleman, K. P. Pre-Validation of an in Vitro Skin Irritation Test for Medical Devices Using the Reconstructed Human Tissue Model EpiDerm^TM. *Toxicol In Vitro* **2018**, *50*, 407–417. DOI: 10.1016/j.tiv.2018.02.007.

(65)   Kugelberg, E.; Norström, T.; Petersen, T. K.; Duvold, T.; Andersson, D. I.; Hughes, D. Establishment of a Superficial Skin Infection Model in Mice by Using Staphylococcus Aureus and Streptococcus Pyogenes. *Antimicrob. Agents Chemother.* **2005**, *49* (8), 3435–3441. DOI: 10.1128/AAC.49.8.3435-3441.2005.

(66)   Kim, J.; Kim, B. E.; Ahn, K.; Leung, D. Y. M. Interactions Between Atopic Dermatitis and Staphylococcus Aureus Infection: Clinical Implications. *Allergy Asthma Immunol. Res.* **2019**, *11* (5), 593–603. DOI: 10.4168/aair.2019.11.5.593.